INVESTIGATION OF ELECTRODEPOSITED CUPROUS OXIDE THIN FILMS

by

EMMA L. MORTENSEN

A dissertation submitted to the

Graduate School- New Brunswick

Rutgers, The State University of New Jersey

In partial fulfillment of the requirements

For the degree of

Doctor of Philosophy

Graduate Program in Materials Science and Engineering

Written under the direction of

Dr. Dunbar P. Birnie, III

and approved by:

_____

_____

_____

_____

New Brunswick, New Jersey

October, 2016

ABSTRACT OF THE DISSERTATION

Investigation of Electrodeposited Cuprous Oxide Thin Films

By EMMA L. MORTENSEN

Dissertation Director:

Dr. Dunbar Birnie, III

This dissertation focuses on improvements to electrodeposited cuprous oxide as a candidate for the absorber layer for a thin film solar cell that could be integrated into a mechanical solar cell stack. Cuprous oxide (Cu_2O) is an earth abundant material that has a bandgap of ~2 eV with absorption coefficients around 10^2-10^6 cm^{-1}. This bandgap is not optimized for use as a single-junction solar cell, but could be ideal for use in a tandem solar cell device. The theoretical efficiency of a material with a bandgap of 2.0 eV is 20%. The greatest actual efficiency that has been achieved for a Cu_2O solar cell is only 8.1%. For the present work the primary focus has been on improving the microstructure of the absorber layer film. The Cu_2O films were fabricated using electrodeposition. A seeding layer was developed using gold (Au); which was manipulated into nano-islands and used as the substrate for the Cu_2O electrodeposition. The films were characterized and compared to determine the growth mechanism of each film using scanning electron microscopy (SEM). X-ray diffraction (XRD) was used to establish and compare the chemical phases that were present in each of the films. The

crystal structure of the Cu_2O film grown on gold was explored using transmission electron microscopy (TEM), and this helped confirm the effect that the gold had on the growth of Cu_2O. The Tauc method was then used to determine the bandgap of the films of Cu_2O grown on both substrates and this showed that the Au based Cu_2O film was a superior film. Electrical tests were also completed using a solar simulator and this established that the film grown on gold exhibited photoconductivity that was not seen on the film without gold. In addition, for this thesis, a method for depositing an n-type Cu_2O film, based on a Cu-metal solution-boiling process, was investigated. Three forms of copper were tested: a sheet of copper, electrodeposited copper, and sputtered copper. The chemical phases were observed using XRD, microstructure was examined using SEM, and the electrical properties were tested using a hot probe test. The sputtered copper turned out to be the most stable film so it was used as the n-type in a homojunction solar cell with the p-type electrodeposited Cu_2O. Recommendations for future experimentation with Cu_2O film development, to improve upon the films and our understanding of the material are included.

ACKNOWLEDGMENTS

I am incredibly grateful for the support that I received from my advisor Dr. Dunbar Birnie. The trust that he put in me and the guidance he gave me throughout this journey has given me the confidence to continue pursuing my goals and reach even higher.

I would like to thank my committee members: Dr. Deidre O'Carroll, Dr. Lisa Klein, Dr. Allen Bruce and Dr. Frederic Cosandey for their input, critique and evaluation of my work.

Thank you to all of my department members that have been by my side through classes and this research. I would specifically like to thank my fellow group members past and present: Sean Langan, Ross Rucker, Josh Epstein, Vishnu Vijayakumar, and Brian Viezbicke. I am very thankful for the undergraduate students that have put so much of their time into this research, specifically: Jenny Coulter, Aishwarya Limaye, Joseph Csakvary, Janki Patel and Tara Nietzold. I would also like to thank all the undergraduate students that have passed through DELLC that I have had the pleasure of mentoring, their excitement for their new journeys in engineering has inspired me more than anything else.

Thank you to Rutgers Materials Science and Engineering Department for the funding I received during my time here from the McClaren and the IGERT Fellowships. Specifically, I would like to thank Dr. Lisa Klein for her assistance throughout my time at Rutgers, and Nahed Assal, Claudia Kuchinow, and Sheela Sekhar for their help with the administrative side of obtaining this degree.

I would like to send a very special thank you to my parents, sisters, grandparents and all of my friends that have stood by my side throughout this journey. I would like to thank them all for their support, patience and belief in me. Finally, I would like to thank my husband Patrick for his unconditional love and support, especially through these final steps, his unwavering confidence in me has made all the difference.

TABLE OF CONTENTS

TABLE OF FIGURES

LIST OF TABLES

CHAPTER 1

1. Introduction

1.1 Global Energy Statistics

As of 2005 energy consumption for the world was at a steady 13 terawatts with 85% of that energy from fossil fuels. The use of fossil fuels has led to an increase of carbon dioxide in our atmosphere, and we have reached the highest CO_2 level in 125,000 years.[1] Without intervention these levels will continue to grow and become unstable and unsustainable by 2050.[2] The U.S. Energy Information Administration has predicted that the world's energy consumption will increase by 56% from 2010 to 2040. This growth is coming primarily from non-OECD countries.[3] Due to this projected growth, and the global concern of climate change, there has been an increased push toward renewable energy sources. As of 2012 21% of world energy generation came from renewable sources such as solar, geothermal, and wind.[4] This use of renewable energy is predicted to increase to 25% by 2040.[3]

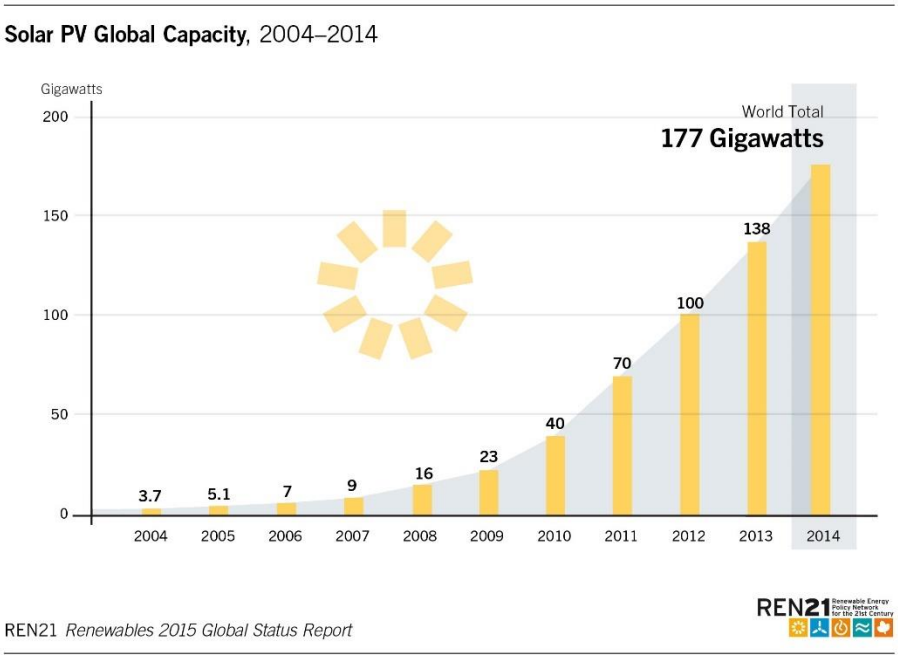

Figure 1.1 The global power capacity for photovoltaics.[5]

Solar energy is on the rise. There is less backlash about the geopolitical, environmental, concerns from the public for this energy source compared to other renewable sources like nuclear or wind. As efficiencies rise and costs lower, solar is becoming a more viable option. As of 2014 there was a capacity of 177 GW for photovoltaics worldwide, this is almost 50 times more global power capacity compared to that of the capacity in 2004 (figure 1.1).

Every hour 100,000 TW of solar power hits the earth's surface; this is enough energy to cover every person's energy requirements for a year.[6] Low cost, and highly efficient solar cells are required to use this sun light effectively. Due to price decreases in panels, solar energy usage has increased; it now covers 1% of the global energy

demand.[7] Solar energy is still only a small part of the global energy sector, which suggests there is room for growth, and that improvements still need to be made.

The National Renewable Energy Laboratory report includes efficiency records that have been set in the different areas of solar cell research: multi-junction cells, single-junction gallium arsenide cells, crystalline silicon cells, thin film cells, and emerging PV. This data is depicted in figure 1.2

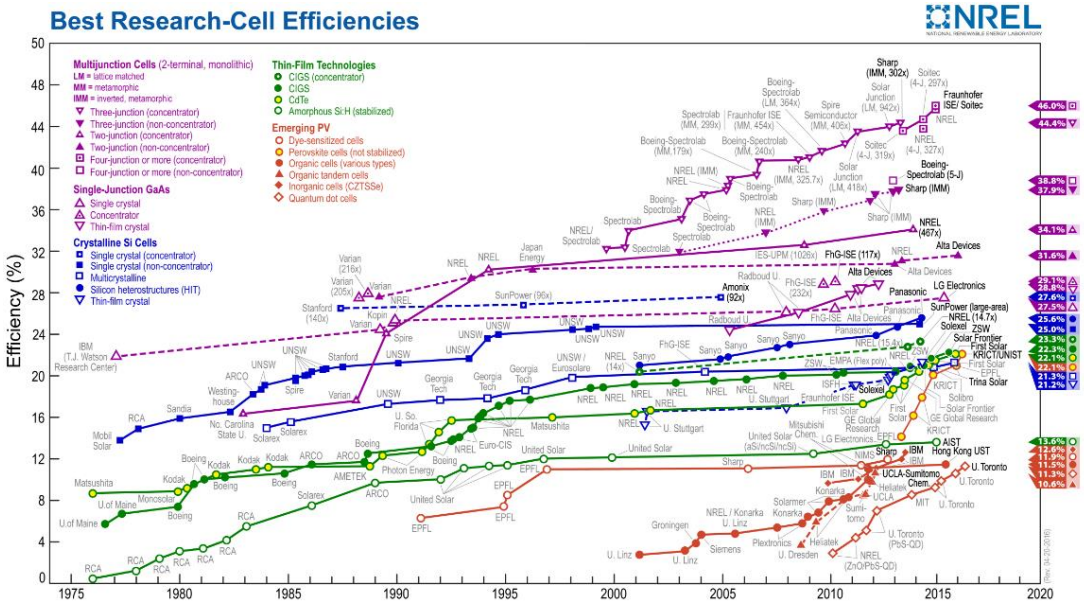

Figure 1.2 NREL research photovoltaic efficiencies records categorized by solar cell type[8]

The NREL report includes data from concentrator (CPV) and non-CPV devices. The CPVs use concentrating optics that allow for solar cells with reduced area.[9] Concentrators are used when the film material is expensive and/or not earth abundant. These cells have the highest reported efficiencies from NREL, but in addition to their expense, these materials are also commonly toxic. The focus of this research is to

develop another option that uses non-CPVs with earth abundant materials, that is competitive with cost and efficiency.

1.2 Background of Photovoltaics

Photovoltaic conversion requires a number of steps: first, a photon from the sun is transferred to the photovoltaic device; then the photon is absorbed into the cell and induces a transition across the bandgap of the semiconductor material that makes up the solar cell; at this point two groups of charge carriers, electron-hole pairs, are created and extracted to separate contacts where the electrical circuit is completed. The electron-hole pair can also recombine and create a phonon that will result in heat. To create a single junction solar cell four parts are required: a front contact, a p-type material, an n-type material, and a back contact. A p-type material results from a deficiency of valence electrons resulting in holes, and an n-type material results from extra electrons in the conduction band. This can be an intrinsic characteristic of the material or a result of doping. The p- and n-type material can be the same material with different dopant or two different materials. When the p-type and n-type materials come in contact this is called a p-n junction, at the interface a depletion region is formed where some of the electrons from the n-type fill in some of the holes in the p-type and this creates an electric field so current can flow.

1.2.1 Energy Loss

Unfortunately, due to the broadness of the solar spectrum there are intrinsic energy losses in a solar cell that cannot be corrected. As a result of these losses, the

maximum efficiency that can be reached for a solar cell is around 35%, as illustrated in figure 1.3. This maximum is known as the Schokely-Quiesser (SQ) limit and this exists because of the trade off between current and voltage.

A material with a narrow bandgap will have energy loss resulting from relaxation to band edge, where the photon energy exceeds the bandgap energy, so all the excess photon energy is lost and converted to heat. This type of material has a larger current and a lower voltage. A material with a wide bandgap has energy loss due to below bandgap photons, where the photon energy is less than the bandgap energy and the

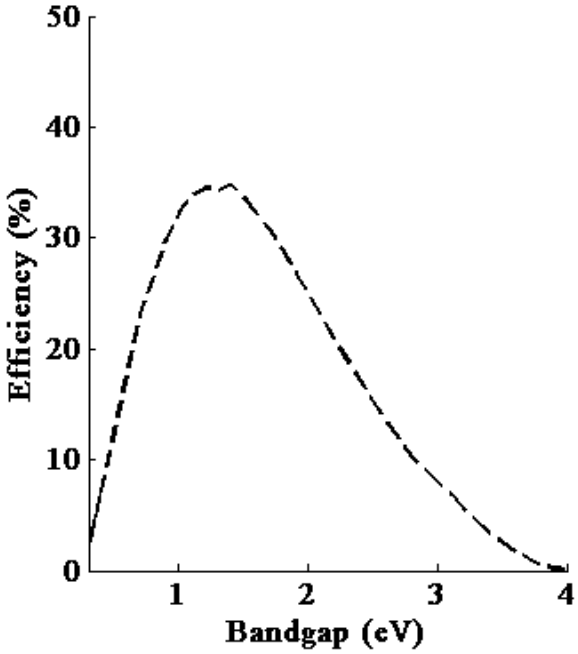

Figure 1.3 Intrinsic efficiency limit for single junction solar cell.[10]

photon is not absorbed. This type of material in a solar cell has a higher voltage and lower current. These energy losses can be seen in figure 1.4. The balance of the voltage and current occurs at the maximum point of the SQ limit at a bandgap of 1.1 eV, and this is the bandgap for silicon. Silicon solar panels are the most common and

commercially available, this type of panel has a theoretical efficiency around that maximum of 35%, however the actual efficiency of these panels has been reported at around 25%, which is shown back in figure 1.2, represented by the solid blue squares.

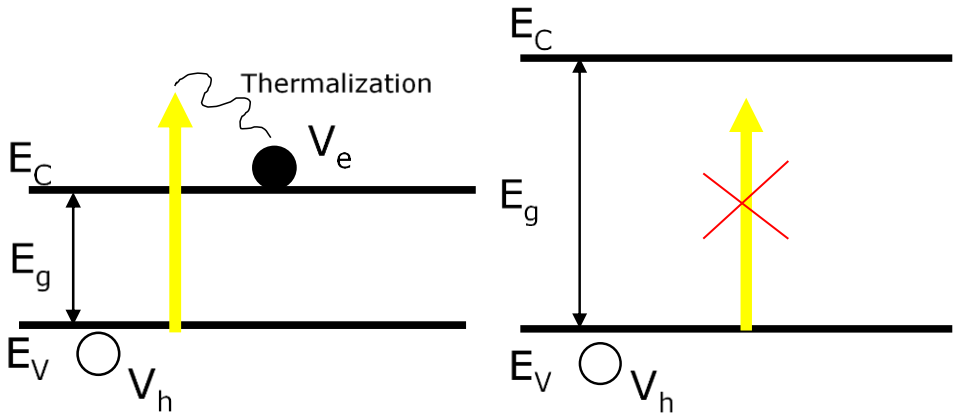

Figure 1.4 Comparison of energy losses from narrow bandgap materials (left) and wide bandgap materials (right)

The difference between the theoretical and experimental efficiencies is due to losses other than the ones represented in figure 1.4, such as recombination. Recombination commonly occurs at grain boundaries, which is a problem for polycrystalline materials used in solar cells, particularly for thin film photovoltaics.[11]

The basis for the present research is to surpass the theoretical efficiency of a single-junction solar cell by layering two solar cells and creating a tandem solar cell. This would minimize the losses that are present in all solar cells because the layering strategy will allow wider energy photons to be absorbed first and then the below bandgap photons to be transmitted to the cell below thus limiting the loss from the relaxtion to band edge. Toward this goal, this research has focused on developing the

top layer of this tandem solar cell, which is a thin film photovoltaic made from cuprous oxide (Cu_2O).

1.2.2 Thin Film Photovoltaics

Thin film solar cells have been investigated since the 1970s. The three most common thin film photovoltaics are cadmium telluride (CdTe), copper indium gallium selenide (CIGS), and amorphous silicon. Some benefits for this type of solar device are, they can be made to be flexible, and they do not use as much material so they are cheaper

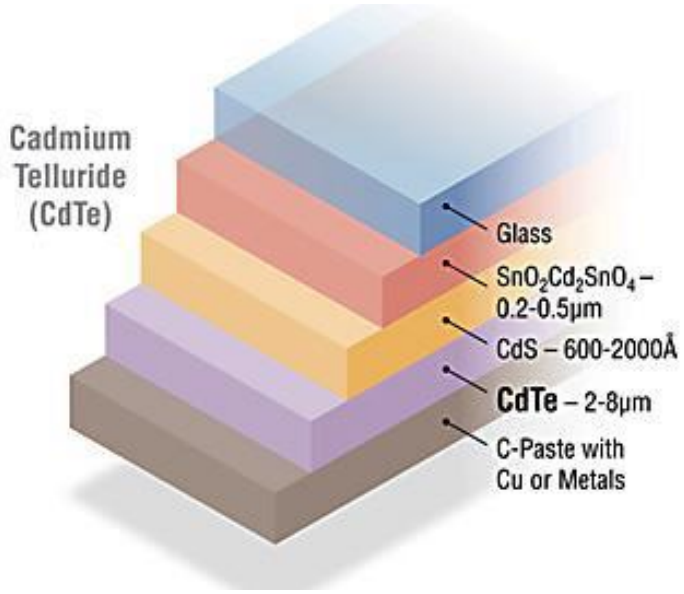

Figure 1.5 Cadmium Telluride thin film photovoltaic architectural illustration.[12]

to make. The maximum efficiency for a thin film solar cell as reported by NREL(2015), and illustrated previously in figure 1.2, comes from a CIGS solar cell at 22.3%, made by Solar Frontier.

The basic structure of a thin film solar cell consists of the four major parts described earlier: back contact, p-type layer, n-type layer, and a top contact. An example of a thin film solar cell is shown using an illustration of CdTe solar cell in figure 1.5. In this image, the bottom is the back contact, this is traditionally a reflective metal film or paste. This layer is used as a conduction pathway to complete the voltaic circuit. The metal chosen as the back contact requires a work function that is compatible with the semiconductor on top of it allowing for better flow of electrons. The next layer is the p-type absorber layer, followed by the n-type window layer, these two layers form the p-n junction. The p-n junction of a thin film solar cell is only a few microns thick or less. In the case of the CdTe cell in figure 1.5 the n-type material is CdS and the p-type material is CdTe. On top of the n-type layer is a transparent conducting oxide (TCO) layer that is commonly a tin oxide doped with either fluorine or indium, this layer is the top contact that completes the voltaic circuit. There is traditionally glass incasing this solar cell.

1.2.3 **Multi-Junction Solar Devices**

A multi-junction solar device is created by stacking or growing two or more p-n junctions on top of one another. In the configuration shown in figure 1.6, the bandgap of the semiconductor junctions decreases from the top of the multi-junction device to the back side. This configuration allows for the least amount of energy loss because the larger energy photons are absorbed in the top cell, while any below bandgap photons are transmitted and absorbed in the solar cell with the smaller bandgap. This layering of

different bandgaps results in a better use of the solar spectrum compared to a single junction solar cell.[13]

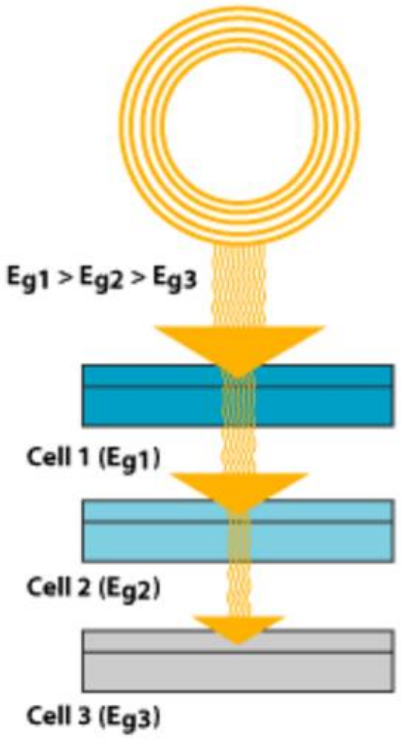

Figure 1.6 Basic multi-layer solar cell architecture.[14]

There are two ways to create a multi-junction solar cell, the first is a monolithic approach where a complete solar cell is made and then the next cell is grown epitaxially on top of the first. With this type of stack there is a current matching constraint. The second type of device is a series of mechanical stacked solar cells. In this case the solar cells are made individually and then adhered together mechanically, there is no current matching constraint in this setup. The most common multi-junction solar cell is made of gallium arsenide (GaAs) in one or all of the layers. GaAs is expensive because it is not an abundant material and it is also toxic, for this reason it is commonly used with a solar concentrator so that less material is required.

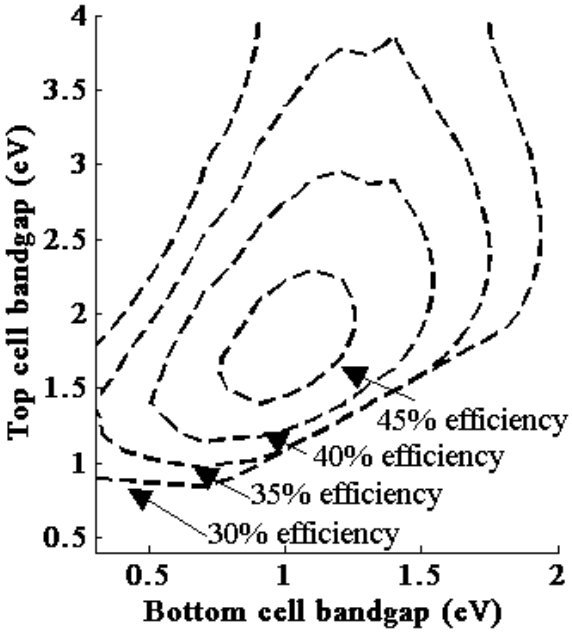

Figure 1.7 Intrinsic efficiency limit of 4-terminal mechanical stack tandem solar cell.[10]

For this research the focus is on a four-terminal mechanical tandem solar cell. Cu_2O is a wide bandgap material, which means it is not optimized for a single junction device based on the SQ limit. However, when paired with silicon in a stacked-tandem architecture, the wider bandgap Cu_2O could be ideal. Figure 1.7 shows a simple derivation of the expected total efficiency using a coupled SQ analysis of this stack, with the maximum efficiency greater than 45% for this stacked design. The architecture would require the top cell to have a bandgap around 2 eV with a bottom cell at 1.1 eV. This stacked theoretical efficiency is based on achieving the individual theoretical efficiencies for each of the two cells. The actual efficiency would be smaller, but the possibility is there that the SQ limit for a single junction silicon solar cell would be

surpassed with the addition of the wide bandgap solar cell on top, and the price would be reasonable due to the low cost of materials and processing. A single-junction silicon

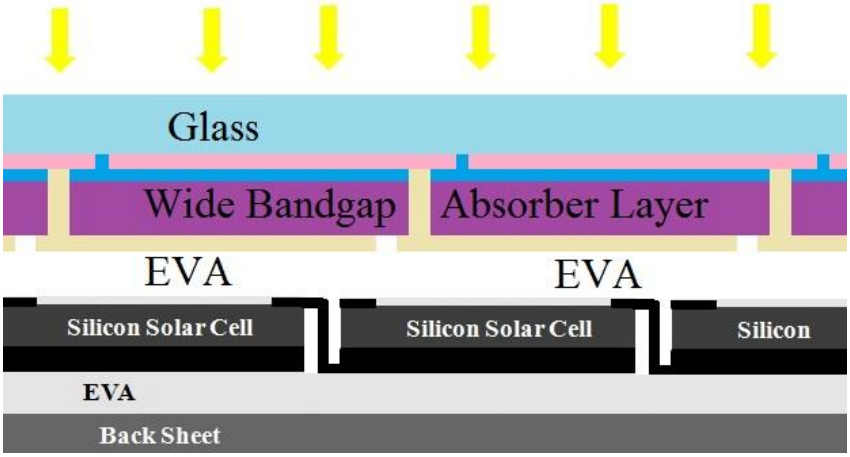

Figure 1.8 Schematic of four-contact tandem solar device with a wide bandgap solar cells on top and silicon solar cells on bottom

solar cell is completed by sealing the panel with a top glass window. To add the top layer, the solar cell would be deposited onto the top glass and then this thin film solar panel would be adhered onto the silicon panel. A schematic of this four-terminal mechanical tandem solar cell is illustrated in figure 1.8.

1.3 Cuprous Oxide Solar Cells

The thin film photovoltaic device that is the focus of this research uses cuprous oxide (Cu_2O). It is believed that the first solar cell to be created was a Cu_2O solar cell made in 1839 by Edmund Becquerel. For this device he used two metal plates submerged in a liquid to produce a continuous current when under sunlight.[15] The conversion efficiency for this archaic solar cell was less than 1%. Cuprous oxide (Cu_2O) has been researched as a viable option for solar power converter due to its high

theoretical efficiency and low cost.[16-20] This theoretical efficiency has been determined using the SQ analysis summarized graphically in figure 1.1 (page 4). Cu_2O with its reported bandgap of around 2 eV, would have a theoretical efficiency of about 20%,[19,21-23] yet the experimental efficiencies for Cu_2O solar cells to date have only achieved an efficiency as high as 8.1%,[24] and before that the efficiency had peaked at 6%.[25] There are two types of solar cells to consider, the first is a homojunction solar cell and the second is a heterojunction solar cell. There have been many studies on both types of solar cell for Cu_2O. Some of the techniques for each kind of solar cell are described below, and a summary of a variety of the Cu_2O solar cells that have been reported on, and their electrical properties, are found in table I.

1.3.1 Heterojunction Cu_2O Solar Cells

Schottky barrier solar cells have been studied extensively with regard to Cu/Cu_2O and are the earliest example of the heterojunction solar cells using Cu_2O. These solar cells are traditionally produced thermally, or in solution, Iwanowski and Trovich developed a technique that uses with hydrogen bombardment to reduce the top layer of a Cu_2O film to Cu.[26] This solar cell works when there is a metal in contact with a semiconductor, at the interface of these two materials there is a highly resistant barrier layer.[16]

In the studies of heterojunction Cu_2O the most common n-type material is ZnO or aluminum doped ZnO (AZO). ZnO is a good choice for the n-type material for this cell because it has a wide bang gap of about 3.3-3.4.[27-30] The layers of this solar cell are commonly electrodeposited one at a time on tin oxide (a TCO) coated glass.[27]

Oxidized copper sheets are also used to produce the Cu_2O films, and the remaining copper is used as the back contact, the n-type ZnO is then deposited using magnetron sputtering.[31,32] Magnetron sputtering has also been used for the Cu_2O layer along with sputtering of ZnO to form the p-n junction.[33-35] Diindium trisulfide (In_2S_3), tin oxide (SnO_2), cupric oxide (CuO), and cadmium oxide (CdO) have also been reported to be used as n-type materials with Cu_2O.[36-39] The Cu_2O solar cell with the highest efficiency of 8.1% was reported by Minami, et al, and is a heterojunction solar cell with $Zn_{1-x}Ge_x$-O n-type.[24]

1.3.2 **Homojunction Cu_2O Solar Cells**

Homojunction Cu_2O solar cells are less advanced than the heterojunction solar cells, and this is due to less understanding and development of n-type Cu_2O. It is believed that the most promising path for increasing the efficiency of Cu_2O solar cells is with a homojunction solar cell.[17] There is some debate on the topic of intrinsic n-type Cu_2O,[40] however there are reports that n-type Cu_2O has been created without dopants.[18,19,41-44] There is also work showing the use of dopants such as fluorine, chlorine, and bromine.[45,46] The efficiencies that have been reported for homojunction Cu_2O solar cells has not reached 1%.

Table I Literature review of Cu_2O solar cells and their electrical properties. [23,24,27,31,32,37,39,43,44,47-53]

Author	Front Contact	P-type (preparation)	N-type	Back Contact	PCE (%)	V_{oc} (V)	J_{sc} ($mAcm^{-2}$)	FF
Papadimitriou	Al	Cu_2O (oxidized Cu)	CdO	Cu		0.4	2	
Georgieva	ITO	Cu_2O (electrodeposition)	ITO			0.34	0.245	
Katayama	SnO_2	Cu_2O (electrodeposition)	ZnO	C paste	0.117	0.19	2.08	0.295
Minami (2004)	AZO	Cu_2O (oxidized Cu)	AZO	Cu	1.21	0.41	7.13	0.42
Han	ITO	Cu_2O (electrodeposition)	Cu_2O	Cr/Au	<0.1			
McShane	ITO	Cu_2O (electrodeposition)	Cu_2O	Au/Pd	0.29	0.423	2.5	0.27
Minami (2011)	AZO	Cu_2O (oxidized Cu)	ZnO	Cu	3.83	0.69		0.55
Hussain	ITO	Cu_2O (electrodeposition)	TiO_2	In	0.15			0.35
Minami (2013)	AZO	Cu_2O (oxidized Cu)	Ga_2O_3	Au	5.38	0.8	9.99	0.67
Kim		Cu_2O (magnetron sputtering)	Si		1.98	0.36	15.2	
Jayakrishnan	Ag	Cu_2O (electrodeposition)	In_2S_3			0.377	0.118	0.33
Minami (2014)	AZO	Cu_2O	Ga_2O_3	Au	5	0.8	11.2	0.6
Hsu	ITO	Cu_2O (electrodeposition)	Cu_2O (pH=4.9)	Al	0.42	0.42	2.68	0.38
Tsai	FTO/Pt	Cu_2O (chemical bath deposition)	I electrolyte	Cu	0.72	0.64	3.52	0.32
Elfadill	ITO	Cu_2O (electrodeposition)	ZnO	Si/Pt	1.445	0.39	9.07	0.41
Minami (2016)	MgF2/ AZO	Cu_2O (Na doped) (oxidized Cu)	$Zn_{0.38}Ge_{0.62}O$	Au	8.1	1.25	11.50	0.7

1.4 Goal of Presented Work

The main goal for this research is to investigate Cu_2O as a possible wide bandgap absorber layer for a mechanical tandem device. The focus was on producing and characterizing a cuprous oxide thin film that can be used as one layer in a tandem solar cell device. The thin film was deposited using electrodeposition, and the deposition technique was modified to produce films that consist of columnar shaped grains. The samples produced using this kind of deposition were characterized to describe their microstructure, composition, optical and electrical properties. Exploration of n-type cuprous oxide was also conducted. The thin film deposition was a two-step process, the first step was a deposition of copper followed by a conversion process from copper to cuprous oxide. This film was then characterized for information about the crystal structure, composition and electrical properties. Solar cells were tested using the p-type Cu_2O on FTO, p-type on n-type, and n-type on p-type layers.

1.5 Breakdown of Thesis Work

Chapter 2 focuses on Cu_2O deposition, and characterization of the resulting films. Two electrolytes were deposited using electrodeposition at different times to understand the deposition process and the grain growth from each solution. These films were then characterized to determine the chemistry and crystal structure.

Chapter 3 discusses the process of microstructural manipulation using gold nano-islands and the analysis of the orientations of the films with the influence of a gold seed layer. These films were analyzed using a transmission electron microscopy (TEM)

scanning electron microscopy (SEM), and x-ray diffraction (XRD). The resulting data and the analysis will be discussed.

Chapter 4 explores the optical properties of the cuprous oxide films specifically focusing on the Tauc analysis to determine the bandgap of the material. Different thicknesses were analyzed to determine if the thickness of the film had an effect on the bandgap as well as the influence of the gold nano-islands on the bandgap.

Chapter 5 looks into the experimental procedures of depositing cuprous oxide in an attempt to produce an n-type Cu_2O layer. It also delves into the characterization of these films to determine the growth process, chemical makeup and the electrical properties of the films that were converted from copper to cuprous oxide.

Chapter 6 provides the conclusions that were drawn from this work.

Chapter 7 discusses the areas where future work might continue based on the work presented in this thesis.

CHAPTER 2

2. Electrodeposition of Cuprous Oxide

2.1 Background of Cuprous Oxide thin film fabrication

As discussed in section 1.2.3, cuprous oxide (Cu_2O) has been researched as a viable option as a solar power converter since the invention of the solar cell, due to its high theoretical efficiency and low cost.[16-20] Experimental efficiencies for Cu_2O solar cells to date have only achieved an efficiency as high as 8.1%.[24] Therefore there is a lot of work that can be done to maximize the experimental efficiency to get closer to the theoretical efficiency mark.

The original method for obtaining a film of Cu_2O was thermal oxidation of copper in air temperatures ranging from 1050^oC[16,54] to 500^oC.[47] Using this method resulted in films of Cu_2O as well as CuO depending on the annealing temperature; the higher temperature was said to produce pure Cu_2O on copper while using a lower temperature between 200^oC-970^oC resulted in a top layer of the CuO film.[54,55] The top layer of CuO had to then be ground off to leave a film of Cu_2O on copper.[47] A similar method from Rosenstock, et al described using a silver layer on top of copper to assist in the diffusion of oxygen at a temperature of 500^oC to obtain a layers Cu/Cu_2O/Ag. This resulted in an extremely thin film of Cu_2O.[56]

Another technique commonly used to deposit a film of Cu_2O is a sol-gel method. In a paper from Ray, et al the deposition is a sol-gel dip technique where the substrate

is dipped into a methanolic solution of copper chloride ($CuCl_2$).[57] Other uses of the sol-gel method rely on using a spin coater to distribute the solution on a substrate.[58-60]

The most promising method for deposition of Cu_2O is electrodeposition because it can be controlled easily, and can be done cheaply. Electrodeposition can be accomplished in a one or two electrode system, where the third electrode is a reference electrode. The elements required for electrodeposition are a working electrode, which is a conduction substrate, a counter electrode, which can be a piece of metal or carbon, a voltage source and an electrolyte solution.[19,27,37,41,44,48,61-68] The first step of this deposition process is the reduction of Cu^{2+} ions to Cu^{+} ions, which is shown in equation 1. The second step is the precipitation of these Cu^{+} ions to form Cu_2O, and this occurs because the ion is not stable. This step is shown in equation 2 and the combination of equations 1 and 2 is shown in equation 3.[18]

$$Cu^{2+} + e^{-} \Longleftrightarrow Cu^{+} \quad (1)$$

$$2Cu^{+} + H_2O \Longleftrightarrow Cu_2O + 2H^{+} \quad (2)$$

$$2Cu^{2+} + H_2O + 2e^{-} \Longleftrightarrow Cu_2O + 2H^{+} \quad (3)$$

Dendritic branching from Cu_2O crystals is common in electrodeposited samples. The dendritic growth occurs when there is a high deposition rate that results in a region of Cu^{2+} around a growing crystal of Cu_2O.[69,70] Once this region is formed, the dendrites will grow faster than the central grain.

The goal of this research is to optimize the growth of Cu_2O as the p-type absorber layer of a solar cell to be used as the top cell of a stacked tandem solar structure with

silicon as the bottom cell. Experimentation for this thesis has focused on improving the microstructure of the Cu_2O layer to improve the efficiency of a Cu_2O solar cell.

2.2 Experimental Reagents

The chemicals that were used for this work are as follows: (i) copper (II) acetate monohydrate, 98.0+% purity, Alfa Aesar purchased from Fisher Scientific; (ii) copper (II) sulfate pentahydrate, greater than 98.0% pure, purchased from Sigma Aldrich; (iii) sodium acetate trihydrate, 99% pure, SigmaUltra purchased from Sigma Aldrich; (iv) sodium hydroxide, 2.5N solution (10%w/v), purchased from Fisher Scientific; (v) sodium DL lactate solution syrup 60% (w/w), synthetic, Sigma Life Science purchased from Sigma Aldrich; (vi) acetone ACS grade, purchased from Fisher Scientific.

2.3 Deposition of Cuprous Oxide

Electrodeposition was used to produce the Cu_2O films. Before the deposition of Cu_2O the substrates were cleaned three times using an ultrasonicator with the substrate in a solution of 2 vol % Micro-90 in DI water, DI water, and finally in acetone. Two chemistries were investigated for the electrolyte solution. The deposition process employed a two electrode, single compartment electrolytic cell that was connected to a tunable voltage source. The working electrode was a piece of FTO coated glass, and the counter electrode was a piece of platinum foil. The first electrolyte (E1) contained 0.02 M copper (II) sulfate pentahydrate, and 0.06 M sodium DL lactate, and six drops of sodium hydroxide were added to bring the solution to a slightly acidic 6.31 pH.[71] The second electrolyte (E2) was made up of 0.1 M sodium acetate trihydrate and 0.1 M

copper (II) acetate monohydrate.[72] The electrodeposition was performed at a potential of 1.5 volts, for various times ranging from 30 seconds up to one hour.

2.4 Characterization

2.4.1 Scanning Electron Microscopy

To characterize these films the Zeiss Sigma Field Emissions scanning electron microscope (SEM) was used to capture images of the surface of the films. Two chemistries were compared after five minutes and after one hour of electrodeposition. The comparisons can be seen in figure 2.1. E1 did not show the flowering microstructure that was expected based on the results from Osherov et al.[71] The structure that resulted from our experimentation was more of a cauliflower structure, however E2 did show the more dendritic grains. We believe that the cauliflower structure was produced because the voltage was higher than what is traditionally used causing overly rapid growth. Both electrolytes produced even coatings.

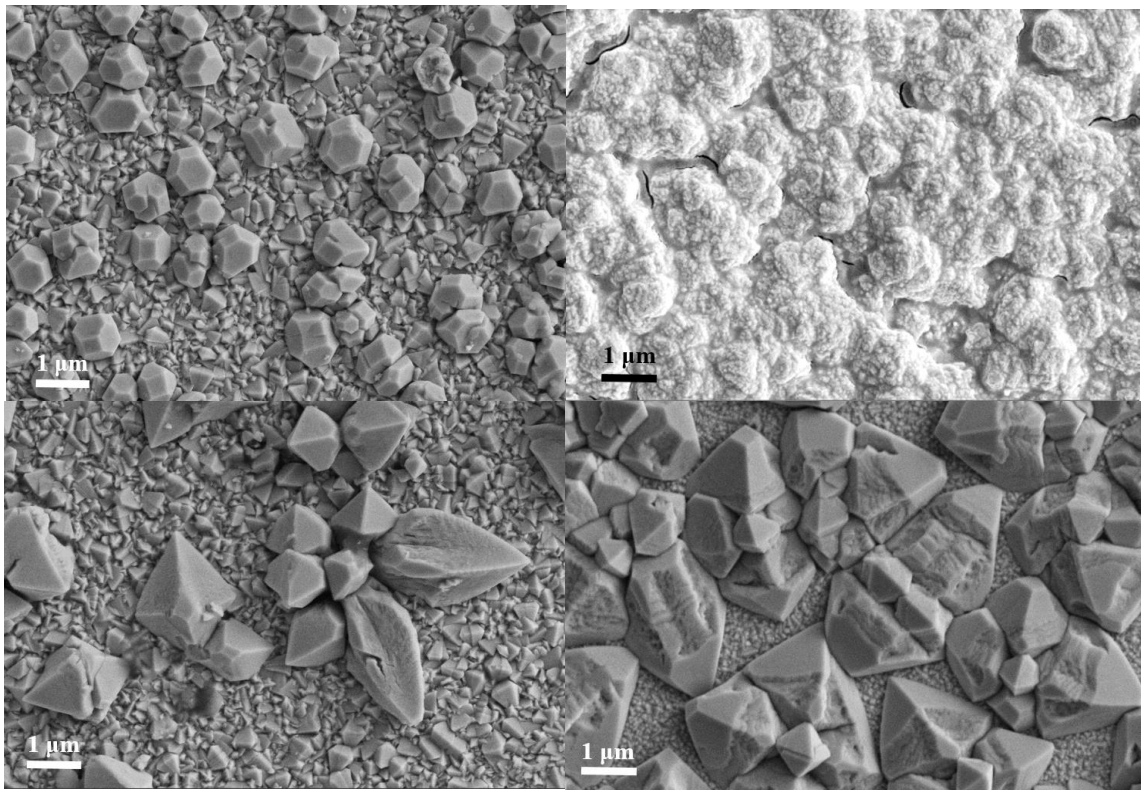

Figure 2.1 SEM images of Cu_2O deposition using electrolyte 1 (top row) and electrolyte 2 (bottom row) electrodeposited FTO coated glass for five minutes, and one hour respectively. All images are at the same size scale.

2.4.2 **X-Ray Diffraction**

X-ray diffraction (XRD) patterns were collected from coatings deposited from E1and E2 on FTO coated glass for one hour of deposition time. The X'pert PANalytic XRD was used for XRD data collection, all of the scans were performed from 20-45º2θ. These patterns can be seen in figures 2.2 and 2.3. All patterns clearly showed the formation of Cu_2O. Trace amounts of copper (Cu) are also present in both XRD patterns. In all cases the FTO substrate peaks are well represented (as noted on the graphs).

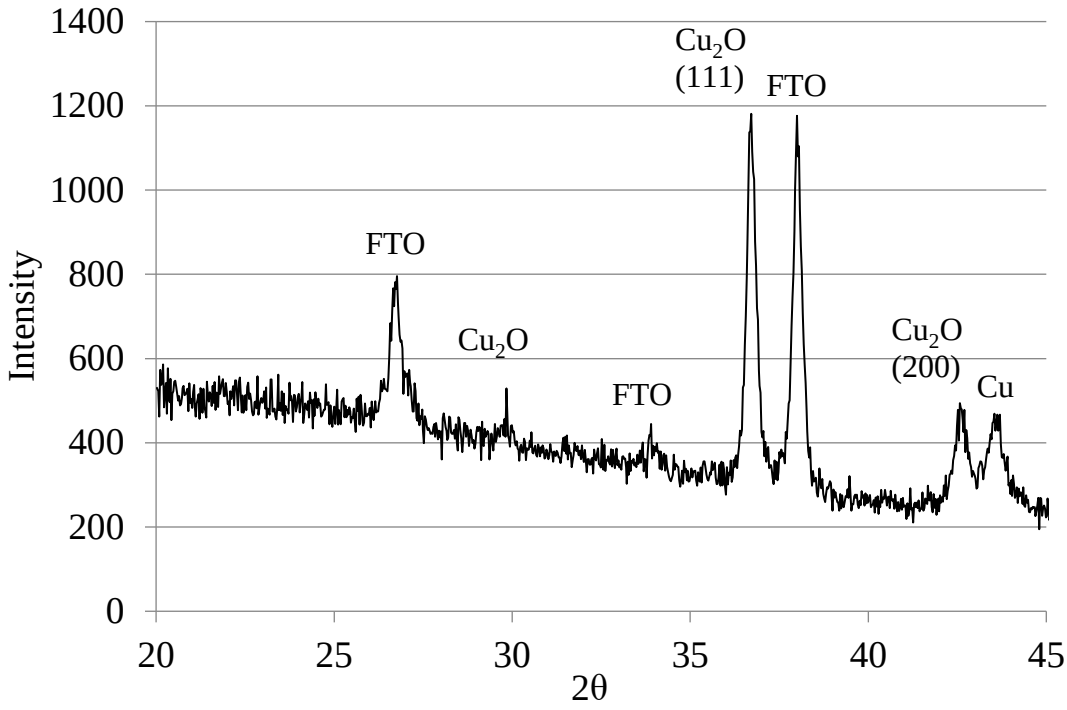

Figure 2.2 XRD patterns for electrolyte 1 electrodeposited for 1 hour on FTO coated glass

For both patterns the most prevalent orientation for Cu_2O are the (111) and (200) directions. The most distinct difference between the patterns of E1 and E2 are the peak heights. When you compare the highest FTO peaks there is a difference of intensity, with E2 being greater by about 400, and for the highest Cu_2O peaks there is a difference of about 300 in intensity, again with E2 having the higher peak.

2.5 Results and Discussion

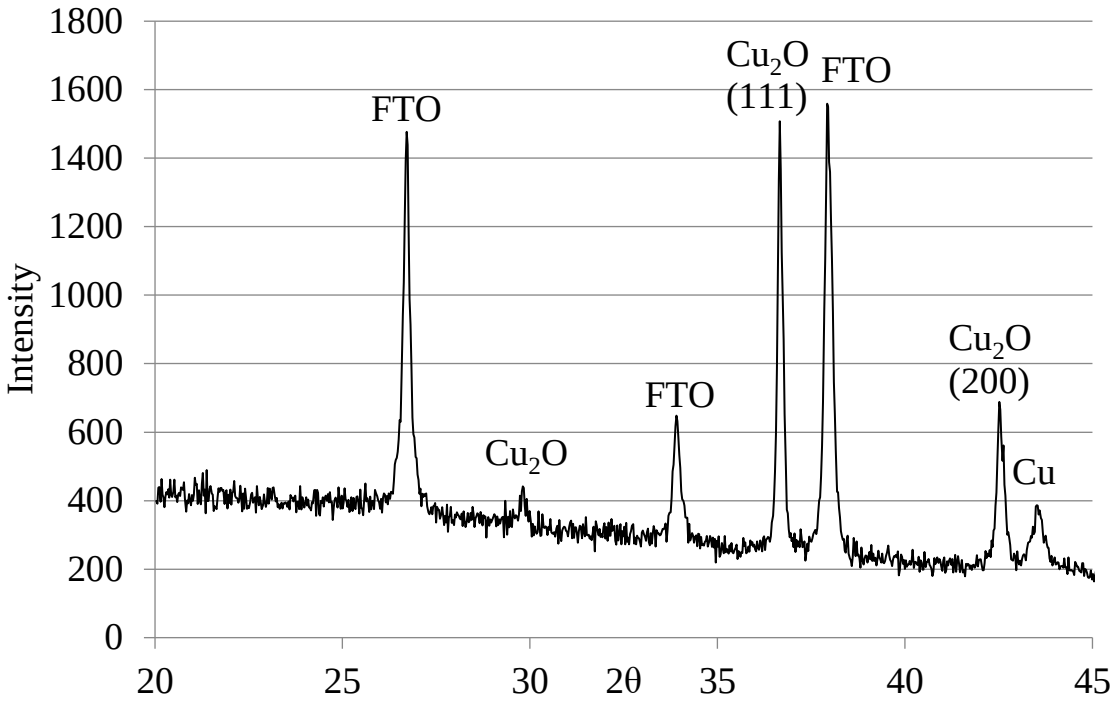

Figure 2.3 XRD patterns for electrolyte 2 electrodeposited for 1 hour on FTO coated glass

Cuprous oxide is a promising semiconductor material with likely value for future tandem solar cells stacks. However, it has been held back in the past by low experimental efficiency in spite of high theoretical expectations based on the bandgap.

Two different electrolytes were used and it was found that E2 was the more desirable of the two, because the growth is more controlled. This electrolyte does grow in a more dendritic/flower-like way and so further research focused on improving this microstructure.

From the XRD patterns that were obtained from these samples it was established that Cu_2O was growing well on the FTO with orientation mainly in the (111) and (200)

directions. Both electrolytes produced Cu, however, the ratio of Cu and Cu_2O is smaller in the E2 film.

CHAPTER 3

3. Orientation Analysis of Cuprous Oxide Seeded with Gold Nano-Islands

3.1 Overview

In the previous chapter it was mentioned that the grains that grow when electrodepositing Cu_2O are primarily dendritic. This is not an ideal grain shape for an absorber layer of a solar cell because it limits the through film pathways for electrons and increases the number of grain boundaries. The density of the film is also a problem with this grain shape; figure 3.1 shows a roughness between the petals of the grains and this roughness is the layer of FTO that the film was deposited on. So the goal of this work is to improve upon the microstructure of the films by focusing on the growth of columnar shaped grains. To do that a technique was employed using a seed layer to encourage growth across the film and in the vertical direction instead of the growth of branches.

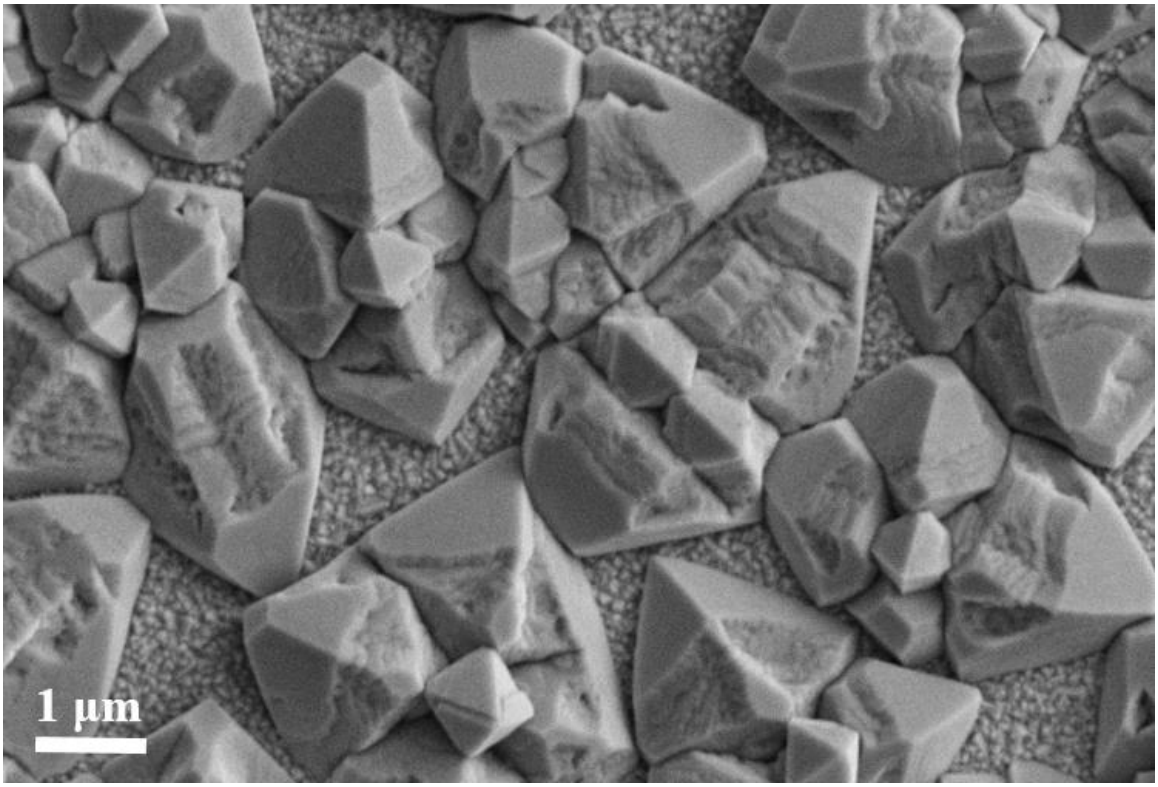

Figure 3.1 Electrodeposited Cu_2O deposited on FTO coated glass.

3.1.1 Background of Gold and Cuprous Oxide

Gold and Cu_2O are paired together frequently in research because of their similar crystal structures. Cu_2O is primitive cubic with a lattice parameter of 0.427nm, and gold is face-centered cubic (fcc) with a lattice parameter of 0.4079nm. The lattice mismatch between these two materials is about 4.7% when using equation 4.[73]

$$(a_{film} - a_{substrate})/a_{substrate} \quad (4)^{[73]}$$

In other research gold has been used to seed the growth of one dimensional nanostructures of materials like GaAs. To produce the nanowires they are grown from the bottom up, a vapor method or solution based method is used to deposit the wire

material.[74] There are examples of a pairing Cu_2O with gold in the literature in the form of a gold substrate,[73,75] or as the core of a nanoparticle[76]. TEM analysis, from a paper by Wang et al, on core/shell relationship between gold and Cu_2O is shown below in figure 3.2. In this image the (111), (110), and (100) are the orientations of the gold facets and the zone axes that are showing are the $[2\bar{2}\bar{2}]$ and $[2\bar{2}0]$. In the images, a5 and b5 arrows point to the two diffraction points that represent the Cu_2O crystal and the Au crystal, they are adjacent to each other. This confirms that the structures and lattice parameters are similar. Also in these images the gold particles are faceted and the Cu_2O matches those facets as the shell on top of the gold core. For this work gold has been researched as a seed layer in the form of nano-islands that can be used in a similar way to grow columnar grains.

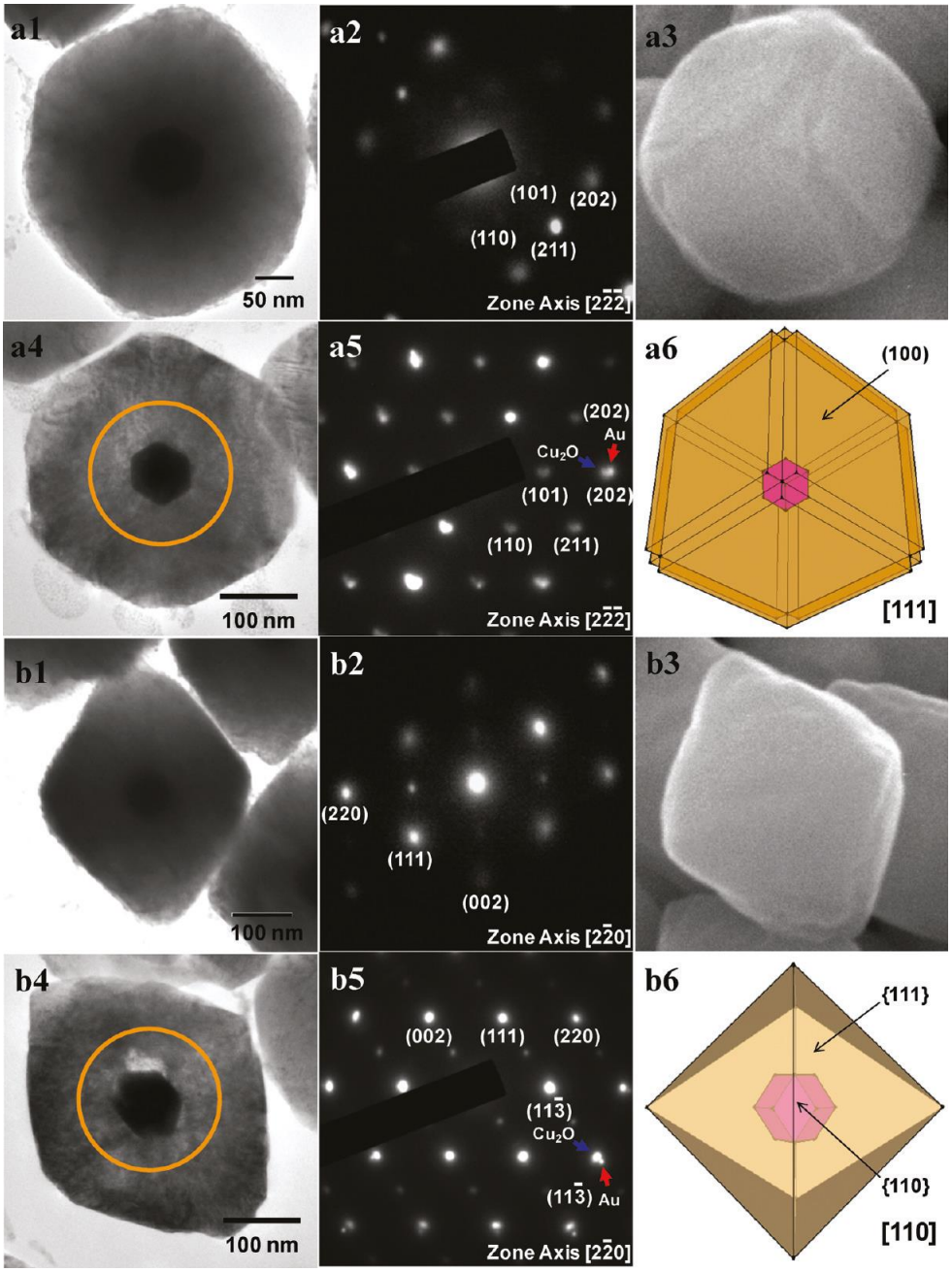

Figure 3.2 TEM characterization of a single Au/Cu_2O core/shell face-raised cube.[76]

3.2 Deposition of Gold Nano-Islands

Gold nano-islands naturally form when a thin layer of gold is deposited on a surface. Before the deposition of the gold, the glass was thoroughly cleaned as described in Chapter 2 using an ultrasonicator three times with the substrate in a solution of 2 volume% Micro-90 in DI water, DI water, and finally in acetone.

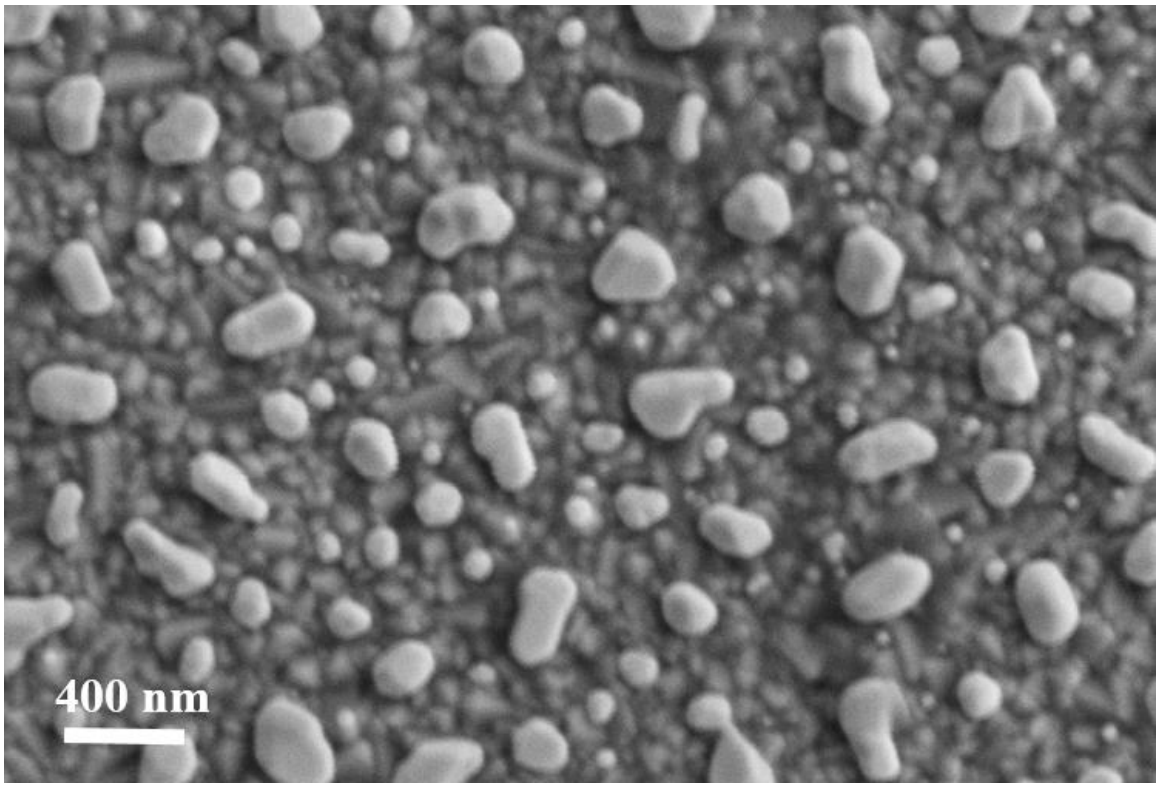

Figure 3.3 FESEM image of gold nano-islands on FTO coated glass, with an average size of 200nm

To obtain the gold nano-islands, gold was sputtered onto the FTO side of the glass, using the EMS 150T ES. In order to expedite the formation of distinct nano-islands the gold coated glass was baked. First the thickness of the gold was explored, 80nm, 50nm, 30nm, 15nm were tested and baked for six hours at 600^{o}C. The 15nm gold film resulted in the most uniform gold nano-islands. Then the bake time was tested, at

four hours, five hours and six hours. From this the six-hour bake was chosen because in the earlier times the gold particles were more elongated, at six hours the particles were the most consistent in size and shape. The resulting gold nanoparticles were an average of 200nm and were evenly distributed on the glass. This can be seen in figure 3.3. The FTO and gold nano-island coated glass was then used as the working electrode in the electrodeposition.

3.3 Deposition of Cuprous Oxide on Gold

The electrodepositon set up for this experiment was the same as described in Chapter 2, which consisted of a two electrode, single compartment electrolytic cell, but in the case of the working electrode it was replaced with the gold coated FTO coated glass. Again we looked at the two electrolytes E1 and E2. E1 contained 0.02 M copper (II) sulfate, and 0.06 M sodium DL lactate, and 6 drops of sodium hydroxide were added to bring the solution to a slightly acidic 6.31 pH.[71] E2 was made up of 0.1 M sodium acetate and 0.1 M copper (II) acetate monohydrate.[72] The electrodeposition was again performed at a potential of 1.5 volts for one hour.

3.4 Characterization

The films were then analyzed and compared to determine the effects of the gold nano-islands on the Cu_2O films. The first characterization technique used was plan-view SEM to understand the surface microstructure of the film. The next area that was explored was the chemical phase identification using the XRD. The orientation relationship between the Cu_2O and the Au was also looked at using TEM. Finally the

electrical properties were compared between the film deposited on Au/FTO and the film deposited on FTO

3.4.1 **Scanning Electron Microscopy**

The Zeiss Sigma Field Emission SEM was used to characterize these films. Images were taken of the Cu_2O samples for the two different electrolytes (E1 and E2) that were deposited on the gold nano-island substrate and compared to those of the samples of Cu_2O deposited on the FTO substrate shown in Chapter 2. The comparisons can be seen in figure 3.4 and figure 3.5. All images were taken at about 29KX magnification.

When deposited on the gold, the Cu_2O film from E2 no longer grew flowering grains but faceted grains. E1 also showed faceted grains compared to the images taken with the FTO substrate. For both electrolytes the grains grown on gold were significantly smaller than those without, and the growth that did occur suggests a more controlled growth when compared to the deposition on just FTO. The gold based growth also encouraged a denser film growth because the rough area (known to be the FTO) that we see in the film grown without the Au does not show in the SEM image of the film deposited on Au.

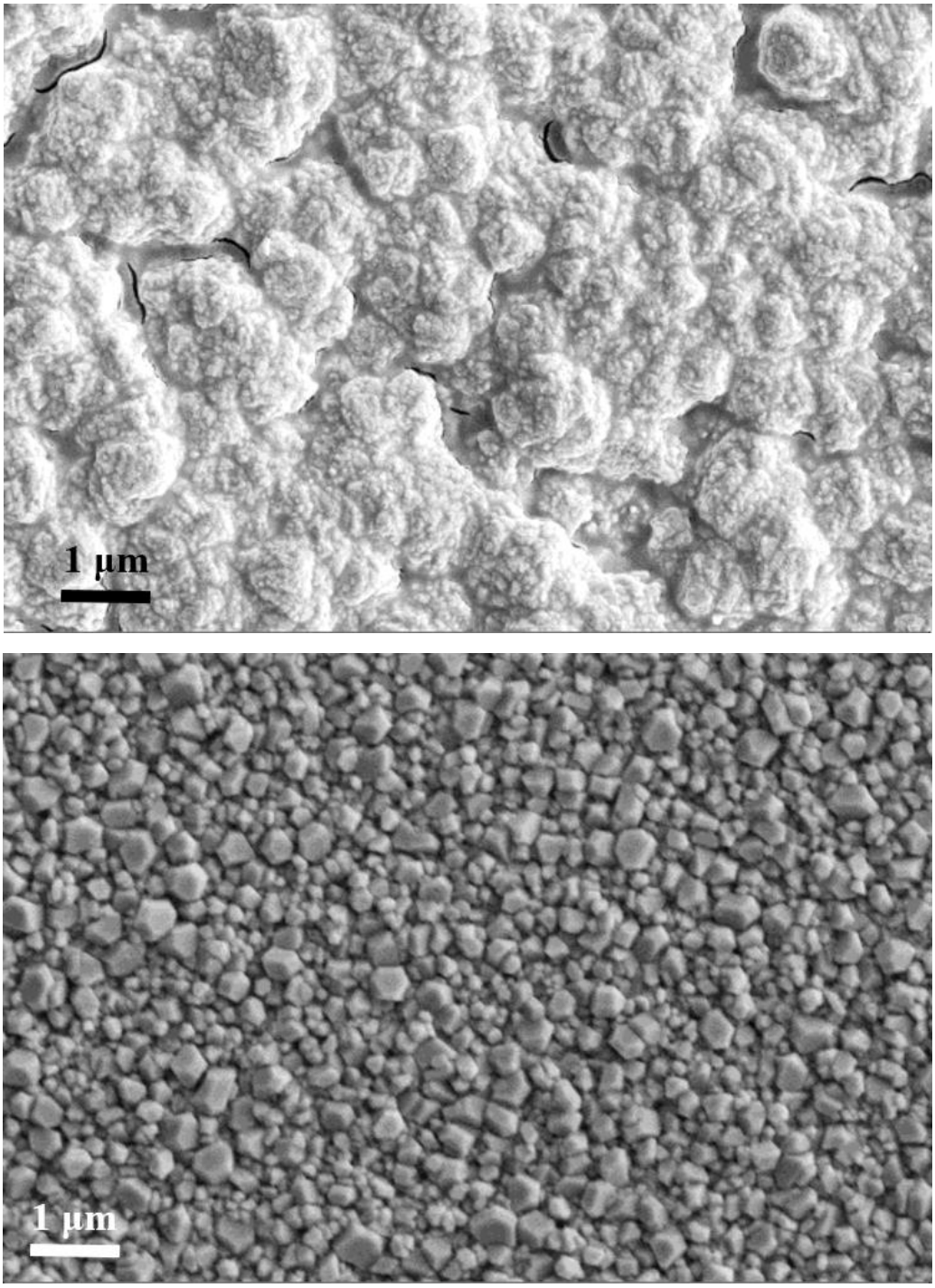

Figure 3.4 SEM images of Cu_2O electrodeposited, using electrolyte 1, onto different substrates FTO (top), and gold nano-island coated FTO (bottom).

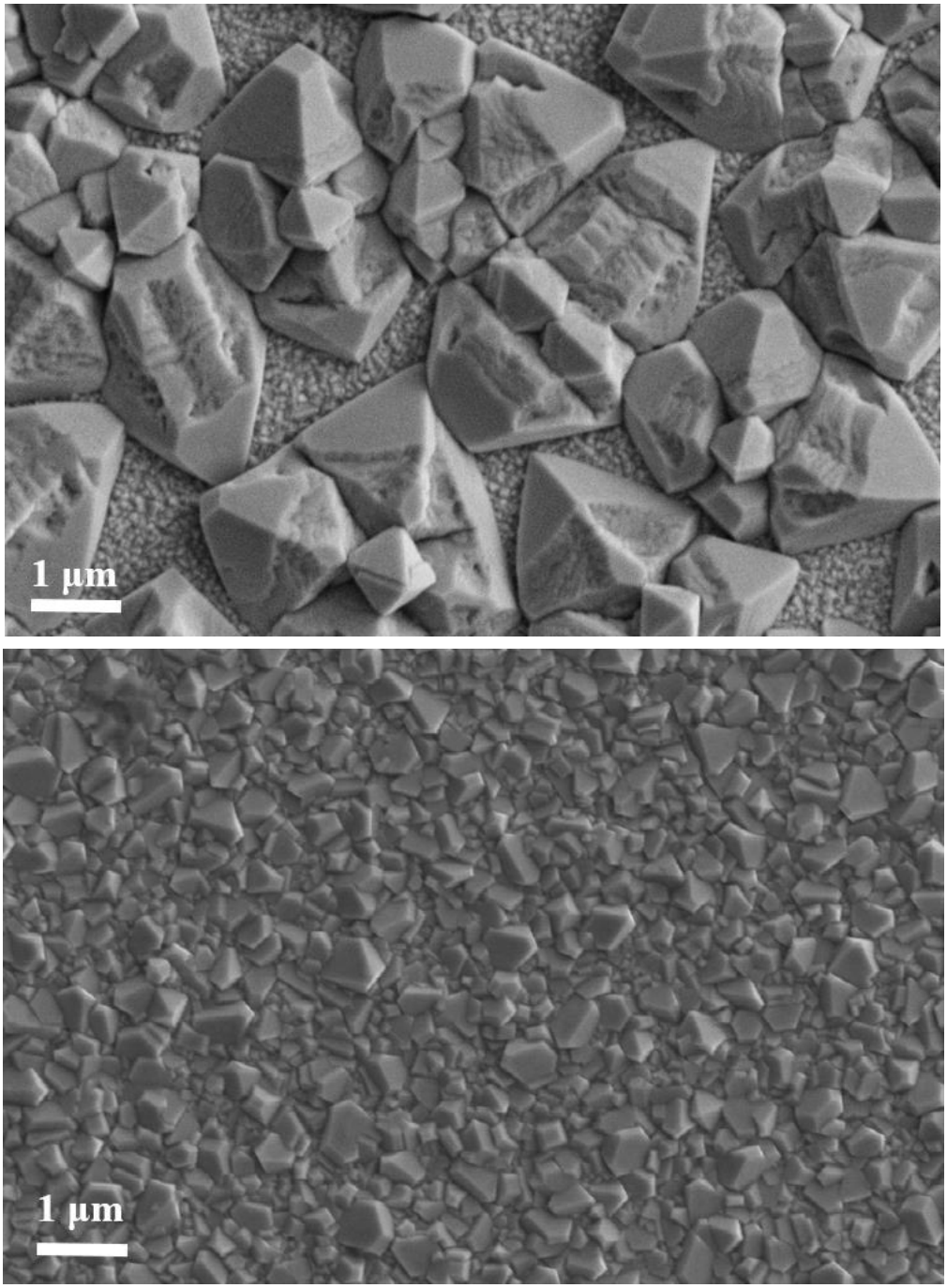

Figure 3.5 SEM images of Cu_2O electrodeposited, using electrolyte 2, onto different substrates FTO (top), and Au nano-island coated FTO (bottom).

3.4.2 **X-Ray Diffraction**

The X'pert PANalytic XRD was also used to compare the E1 and E2 films. As mentioned in the previous chapter traces of copper were found in the films of both electrolytes using the FTO substrate. When E2 was deposited on Au it was found that the traces of copper had almost entirely disappear. However, the samples using E1 examined with XRD, show the copper traces were still present even when gold was added to the substrate.

This comparison can be seen in figure 3.6 and 3.7. The top graph in both figures is Cu_2O deposited on FTO and the bottom graph is for Cu_2O deposited on gold and FTO. Also in both figures there is a decrease in the peaks of the Cu_2O with the addition of gold particularly in the peak representing the (111) orientation. This decrease in Cu_2O is due to a change in thickness when Au is added to the substrate, the film without Au is not as dense and therefore the growth occurs in the vertical direction whereas the growth with Au occurs from the substrate so it is not as thick and the resulting signal for the XRD is not as strong.

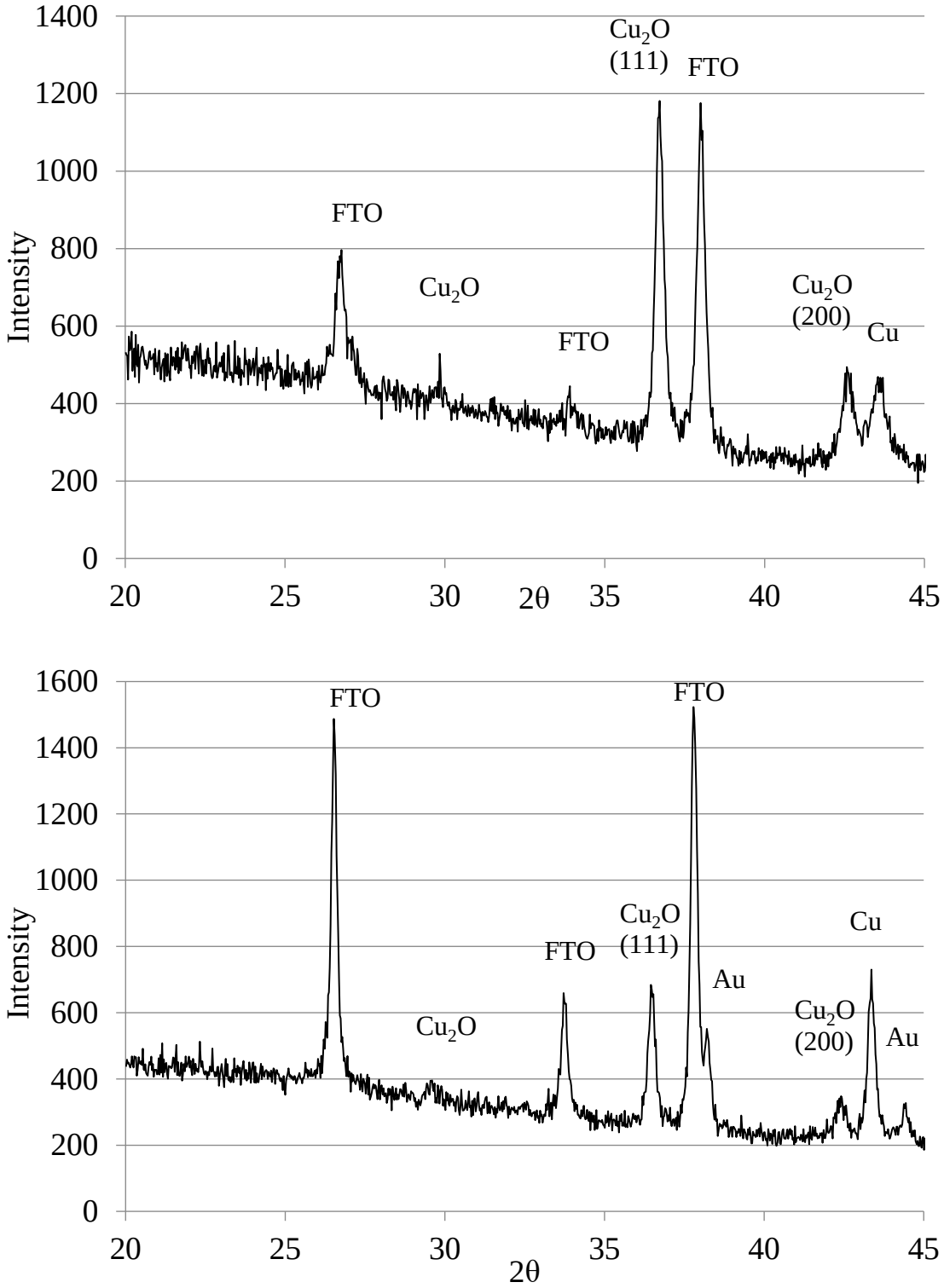

Figure 3.6 XRD pattern comparing electrodeposited Cu_2O on an FTO coated glass substrate (top) and on a gold coated FTO coated glass substrate (bottom). This sample used electrolyte 1

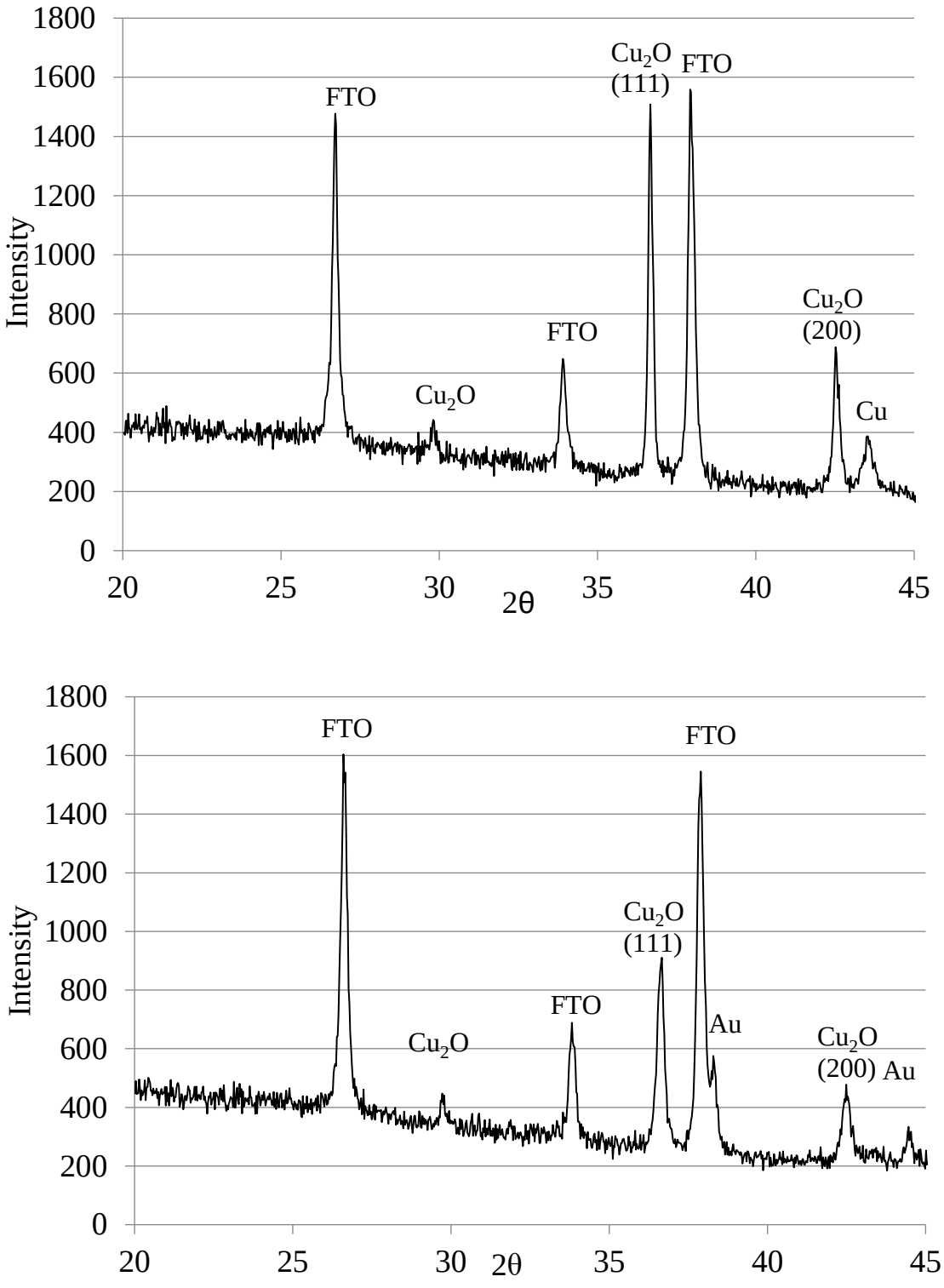

Figure 3.7 XRD pattern comparing electrodeposited Cu_2O on an FTO coated glass substrate (top) and on a gold coated FTO coated glass substrate (bottom). This sample used electrolyte 2

3.4.3 **Transmission Electron Microscopy**

TEM was used to determine whether there was epitaxial growth occurring at the interface of the gold nano-islands and Cu_2O, and a film grown using E2. First a sliver of the film was cut from the sample using a focused ion beam (FIB). This was performed by Evans Analytical Group (EAG) in an FEI Strata 400 Dual Beam FIB/SEM. During this process the ion beam was used to cut away trenches in the sample so that a narrow section could be removed and attached to a sample holder using platinum and thinned using the same ion beam, the thinning is necessary for the TEM analysis. Once the sample was prepared it was analyzed using the FEI Tecnai TF-20 FEG/TEM operated at 200kV in bright-field (BF) TEM mode and high-resolution (HR) TEM mode. The sample was aligned and images were taken. Two of these images are shown in figure 3.8 and 3.9. Both figures are bright field, high resolution TEM image.

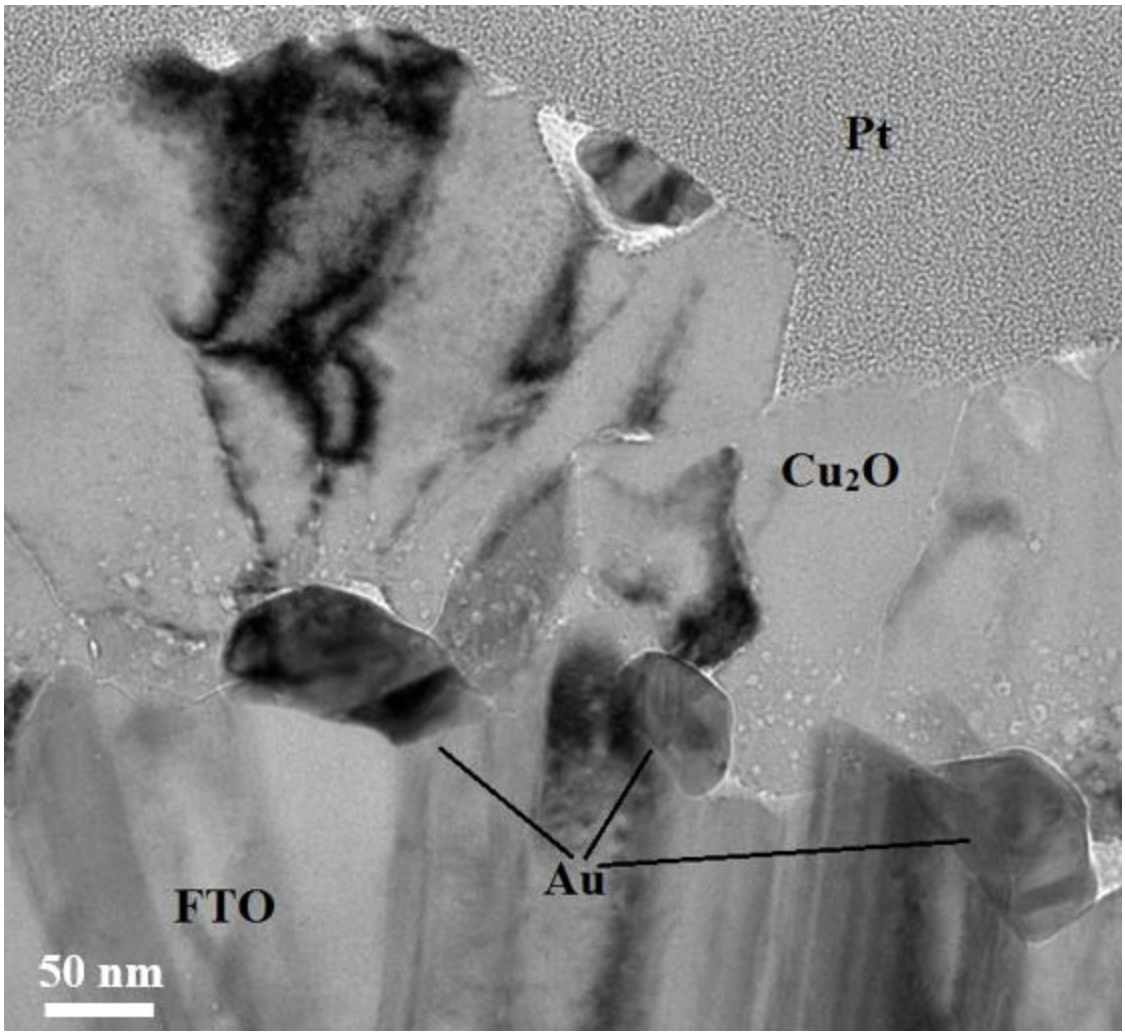

Figure 3.8 HR-TEM showing the cross section of the electrodeposited Cu_2O on gold nano-islands and FTO coated glass. The platinum is present from the process of cutting the sample using FIB.

Figure 3.8 was taken at a magnification of 39KX and shows the full cross section of the film that was produced. The top layer is platinum that was deposited during the FIB process, followed by the electrodeposited layer of Cu_2O, below which are the gold nano-islands. The gold nano-islands are on top of the commercially prepared FTO coated glass. In this image the grains are faceted and are growing vertically in the desired columnar shape.

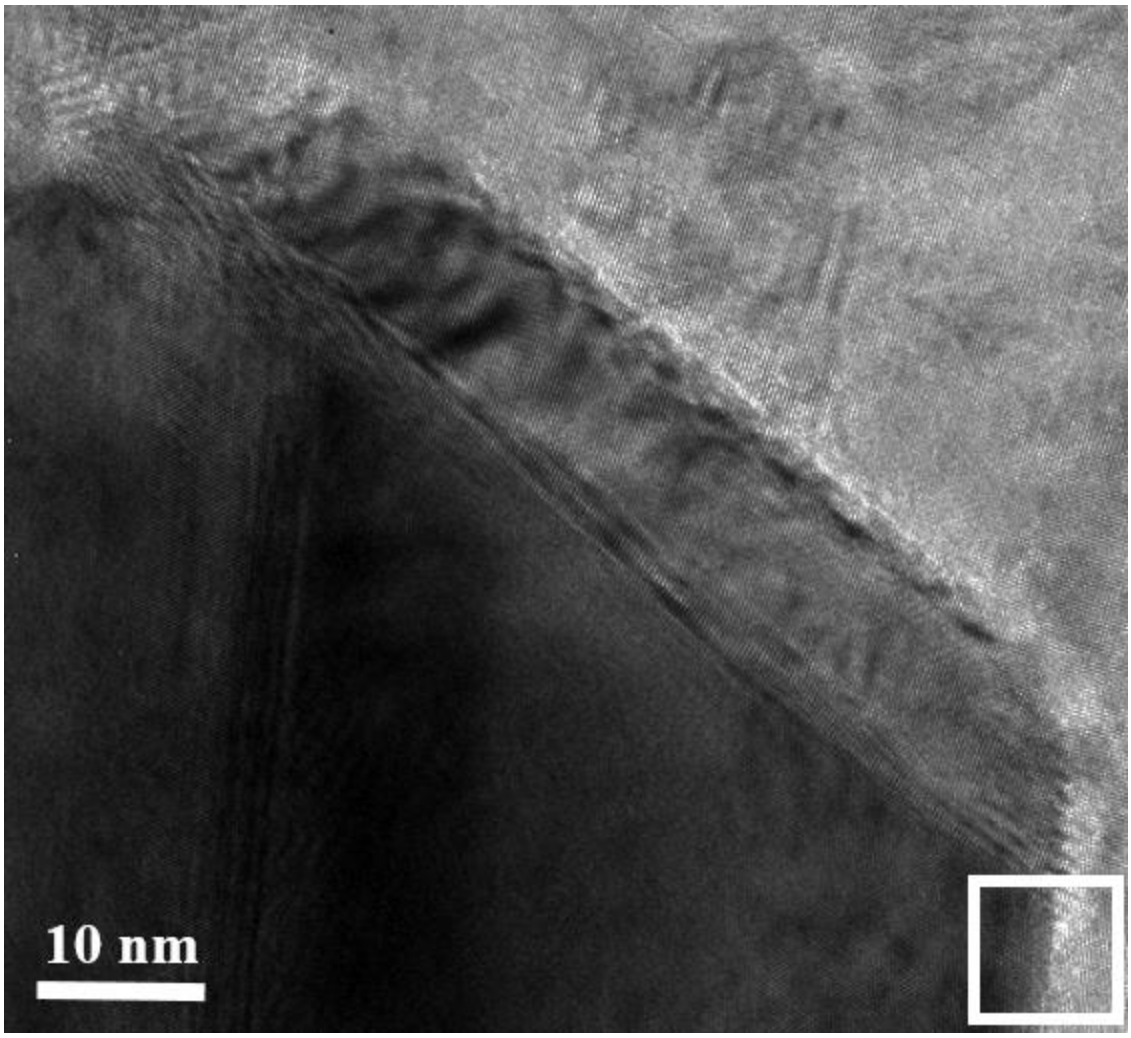

Figure 3.9 HR-TEM magnified image of a gold particle that has Cu_2O electrodeposited on top. The black box highlights the region where a fast Fourier transform was taken.

Figure 3.9 is a high magnification image at 360KX. This image focuses on the interface between the gold particle and the Cu_2O, and at this magnification the lattice fringes are apparent proving that there is high quality crystal growth of the Cu_2O. DigitalMicrograph was then used to get more information from the TEM images, using the fast fourier transform (FFT) function. The white square shown in figure 3.9 is the area highlighted in figure 3.10 shown below. In this region both Cu_2O and gold are represented and they are shown in the figure using arrows. These spots are reminiscent

of the diffraction pattern that is shown in figure 3.2 a5 and b5 where there is a large spot and a small spot very close to one another. The orientation of the spots also matches the diffraction pattern of the six spots that surround the beam blocker in the image from figure 3.2 a5, which indicates that the zone axis in that region of the film is $[1\bar{1}\bar{1}]$.

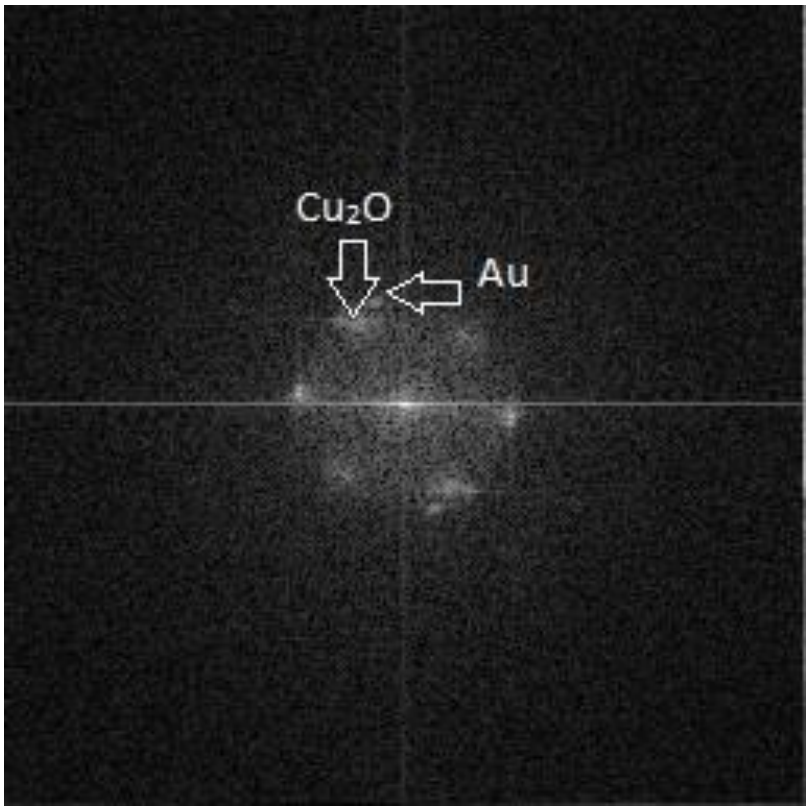

Figure 3.10 Fast Fourier transform of the area highlighted in figure 3.9. The arrows highlight the spots that represent Cu_2O and Au in the pattern.

The next area on figure 3.9 that was analyzed was the center of the diagonal edge of the Au particle. An FFT was taken from this region and then an inverse FFT was taken to get a higher magnification image of the same region, this can be seen in figure 3.11. This images shows the interface between the gold particle which is the

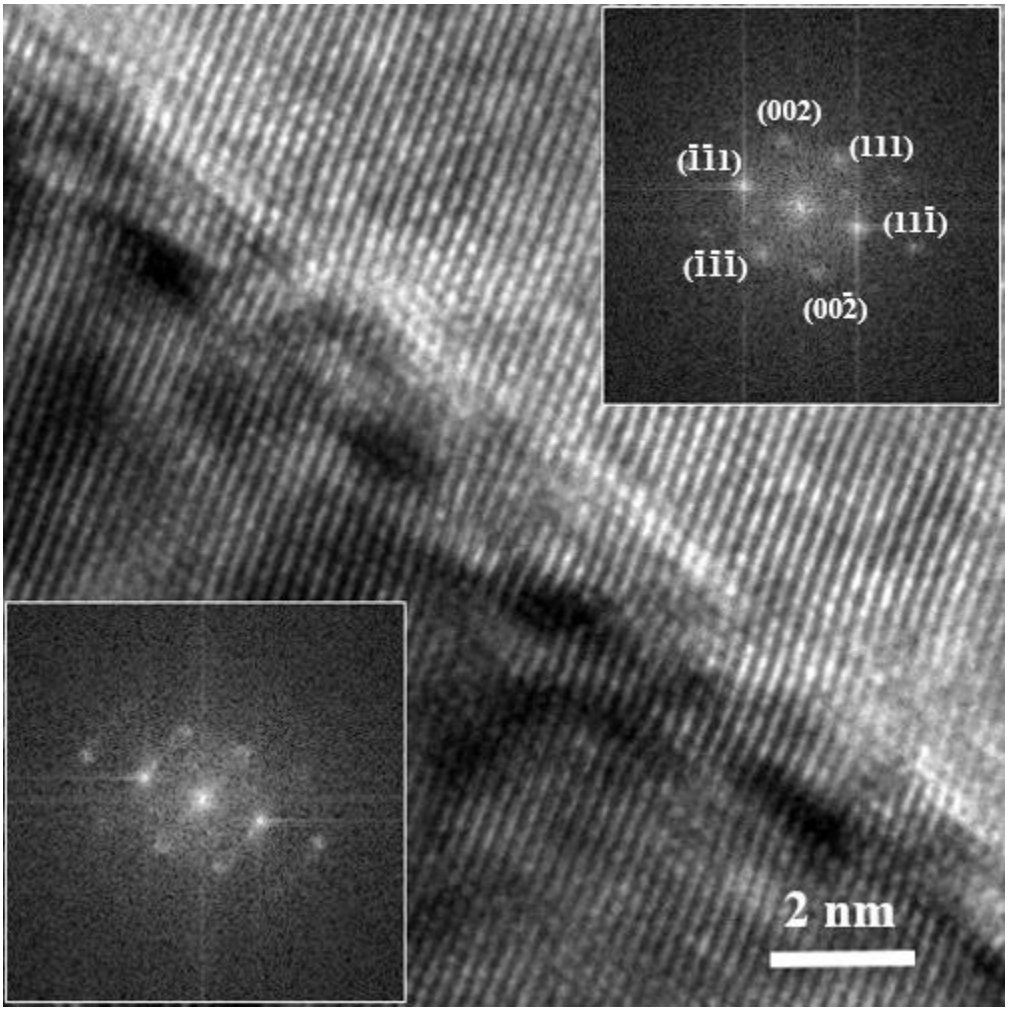

Figure 3.11 Inverse fast Fourier transform of the interface between a gold particle (left side) and Cu2O film (right side) this is from the boxed area highlighted in figure 3.9

the darker region on the left, and the Cu_2O film, which is the lighter region on the right. In the image the lattice fringes can be seen running smoothly between the interface, from the gold particle into the Cu_2O film. Also in this figure the FFT from either side of the interface is overlaid on the corresponding region. In the FFT for the Cu_2O region the diffraction spots have been labeled with Miller indices. This pattern has a zone axis of $[1\bar{1}0]$. The gold has the same orientation and would be indexed the same way. Using figure 3.11 the fringe spacing was measured on the Cu_2O to be 0.253 nm, and this is

consistent with the known Cu_2O lattice spacing of the {111} plane. Finally, the interface between the gold and Cu_2O in figure 3.11 is in the (111) plane, this is known because it is perpendicular to the (111) Miller index from the Cu_2O FFT. This would be one of the lowest energy surfaces of gold.

3.4.4 **Solar Simulation**

A Newport model solar simulator was used to obtain electrical properties from the Cu_2O films that were electrodeposited from E2 for one hour at 1.5 V. As mentioned earlier there is some work that uses tin oxide (SnO_2) as the n-type material for Cu_2O solar cells. This characterization takes the electrodeposited films and tests them in a solar simulator using the FTO substrate as the n-type material as well as the top contact. A device was also made using Cu_2O deposited onto gold on FTO. For the simulation a back contact of Au was sputtered on with a thickness of 60nm. In table I, in section 1.3, Au is a material that has been used as the back contact to a Cu_2O solar cell, The solar simulation was programed to run from -1 volt to 1 volt. Two runs were completed for each sample: one run with the solar simulation light on and one without the light. The simulation results are shown in figures 3.12 and 3.13.

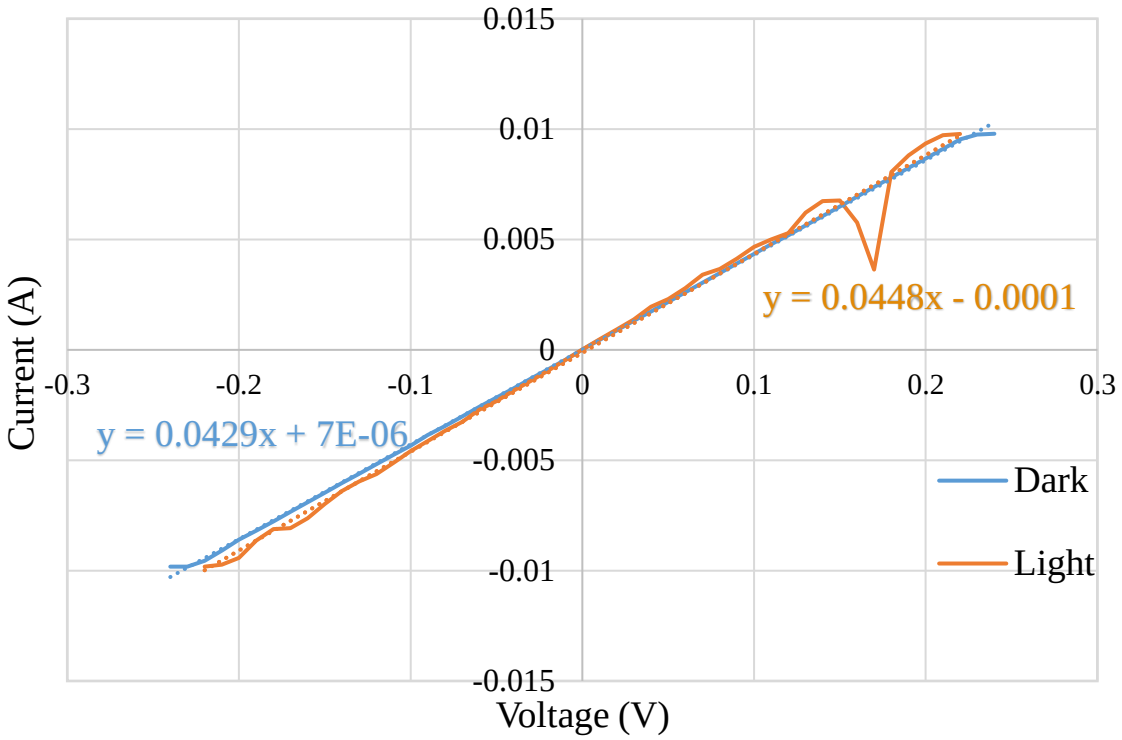

Figure 3.12 Solar simulation data for electrodeposited Cu_2O on an FTO substrate in light (orange) and in dark (blue).

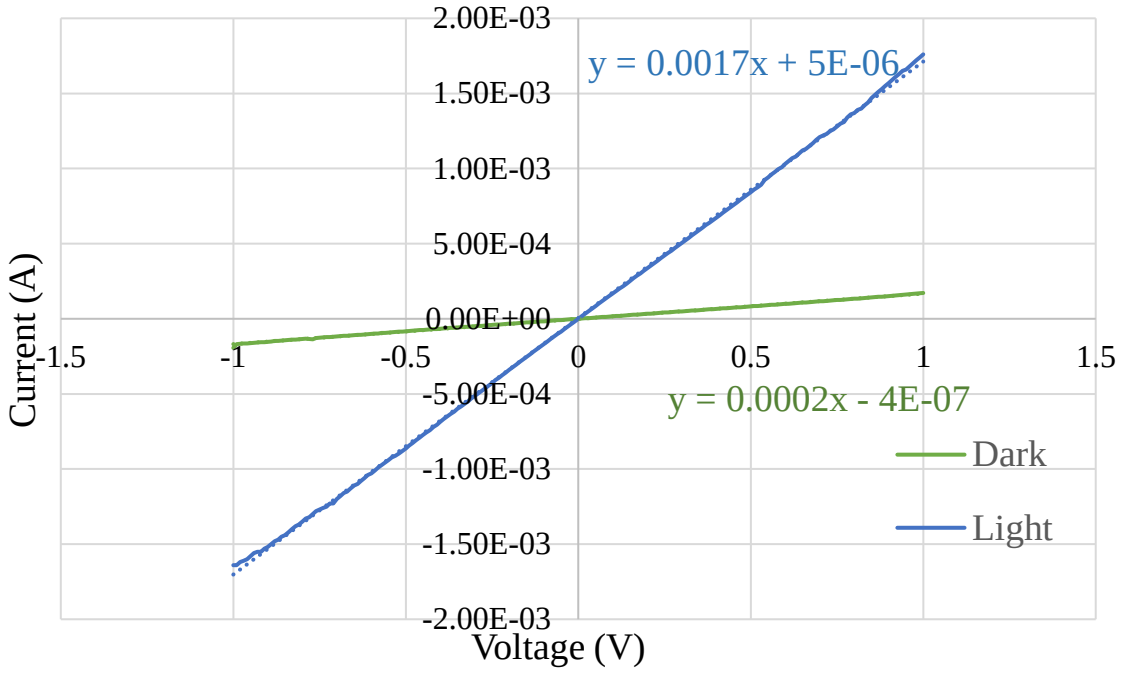

Figure 3.13 Solar simulation data for electrodeposited Cu_2O on an Au/FTO substrate in light (blue) and in dark (green).

3.5 Results and Discussion

From the results of the XRD and SEM we have further concluded that E2 is the best electrolyte for this project. When used in combination with the gold nano-islands the SEM images (figure 3.2) show that the surface is faceted as expected from the Au-Cu_2O nanoparticles, and the dendritic growth that is common in electrodeposited Cu_2O does not occur under the influence of the Au seed particle. With the data from the XRD the E2 film on the seed particle substrate was found to be without the trace amount of copper that was in the films when it was deposited directly on FTO. E1 did not show the elimination of copper with the addition of gold.

When TEM analysis was used on a film of electrodeposited E2 on gold nano-islands the growth of the Cu_2O on the gold nano-islands was found to be epitaxial. The cross sectional image showed columnar shaped grains stemming from gold particles. With further analysis, using the fast Fourier transform and inverse fast Fourier transform features in the DigitalMicrograph software, it has been determined that the diffraction pattern in the Cu_2O and the Au are similar. There is some shifting of the pattern, but the orientations of the two materials is essentially matched, further proving that the gold nano-islands are seeding the growth of the Cu_2O films during the electrodeposition process.

Finally the solar simulation on the p-type electrodeposited Cu_2O and n-type FTO did not result in any photovoltaic properties. This is illustrated by the plot that runs through the origin for each of the samples, in both light and dark. The two types of film, Cu_2O/Au/FTO and Cu_2O/FTO showed markedly different photoconductivity properties. The sample with an Au substrate had an increase in slope with the light on, compared

to the run with the light off; the increase was 10 fold, from 0.0002 Ω^{-1} with the light off to 0.0017 Ω^{-1} with the light on. There was no difference in the slope for the sample without Au between the Cu_2O and FTO layers. This is believed to be due to the conductivity of the film without Au, the slope for I-V plots for the Cu_2O/FTO samples show the same slope, which is about 0.044 Ω^{-1}. This is 22 Ω compared to the resistance of the Cu_2O/Au/FTO under light, which is 588 Ω. The Cu_2O is more resistant, which means that the photoconductivity properties of this film are more apparent compared to the more conductive film (Cu_2O/FTO). The resistivity is calculated using equation 5 where ρ is the resistivity, R is the resistance, A is the area of the film, and t is the film thickness.

$$\rho = RA/t \qquad (5)$$

The resistivity of the film of Cu_2O on Au/FTO in dark was calculated to be 3.36×10^8 Ωcm. This is larger than the resistivity of other Cu_2O films that can range from 76 Ωcm to 2000 Ωcm.[17,47,55,61,68] From the Olsen paper, the Cu_2O is converted from Cu metal and these samples are more strongly reduced showing a much lower resistivity value.[17] Based on the calculated resistivity, the hole concentration was calculated using equation 6, where p is the hole concentration, sigma is the conductivity (inverse resistivity), q is the charge of an electron, μ_h is the hole mobility.

$$p = \sigma/\mu_h q \qquad (5)$$

For this calculation a few assumptions were made, the first is that n equals p and the mobility is equal to silicon. The carrier concentration was calculated to be 8.06×10^7.

CHAPTER 4

4. Optical Properties of Cuprous Oxide

4.1 Background of Bandgap Estimation

The standard bandgap that is reported for Cu_2O is 2.0 eV, however there are some conflicting reports in the literature. The bandgap of Cu_2O has been report ranging from 1.7 to 2.7 eV. These reported numbers and the authors that reported them

Table II Summary of reported bandgaps of Cu_2O and the authors that reported the bandgaps.[18,20,47,48,51,59,61,63,77-79]

Author	Reported Bandgap
Uihlein	2.172
Papadimitriou	2.3
Golden	2.1
Balamurugan	2.33-2.61
Georgieva	2.38
McShane	1.9
Akhavan	1.70-2.7
Gu	2.18
Hussain	2.19
Gupta	2.44
Jeong	1.70-2.53

are shown in Table II. This thesis is based on the idea the Cu_2O is a good candidate for the top cell of a tandem device primarily because the bandgap is frequently reported around 2 eV. Therefore, it was important to confirm the bandgap of the material that

was the basis for this work. UV-Vis spectrometry and the Tauc method were used to put together a Tauc plot for Cu_2O films grown on FTO and Au/FTO.

4.1.1 Cu_2O Band Structure

From a paper by Heinemann et al, the band structure of Cu_2O has been calculated using the density functional theory (DFT). This result is shown in figure 4.1, the band structure is shown in the top image and the bottom image shows the corresponding Brillouin zones for Cu_2O.[80] In the shaded region around the Γ-point of the band structure the two parabolic lines represent the valence band (bottom) and conduction band (top). The gap between these two bands is the bandgap of Cu_2O and in this image it is at about 2.2 eV. Just above the conduction band is another parabolic band and the gap between this band and the valence band is about 2.6 eV. These two gaps are pictured again in figure 4.2, but in this case the only point from the Brillouin zones shown is the Γ-point. In the image it shows the first gap at 2.17eV and the second gap, wider by 0.45 eV, at 2.62 eV. These two bandgaps are described as the direct bandgap (2.17 eV) and the optical gap (2.62 eV)[81] and explains why there is a wide range of bandgaps reported in table II.

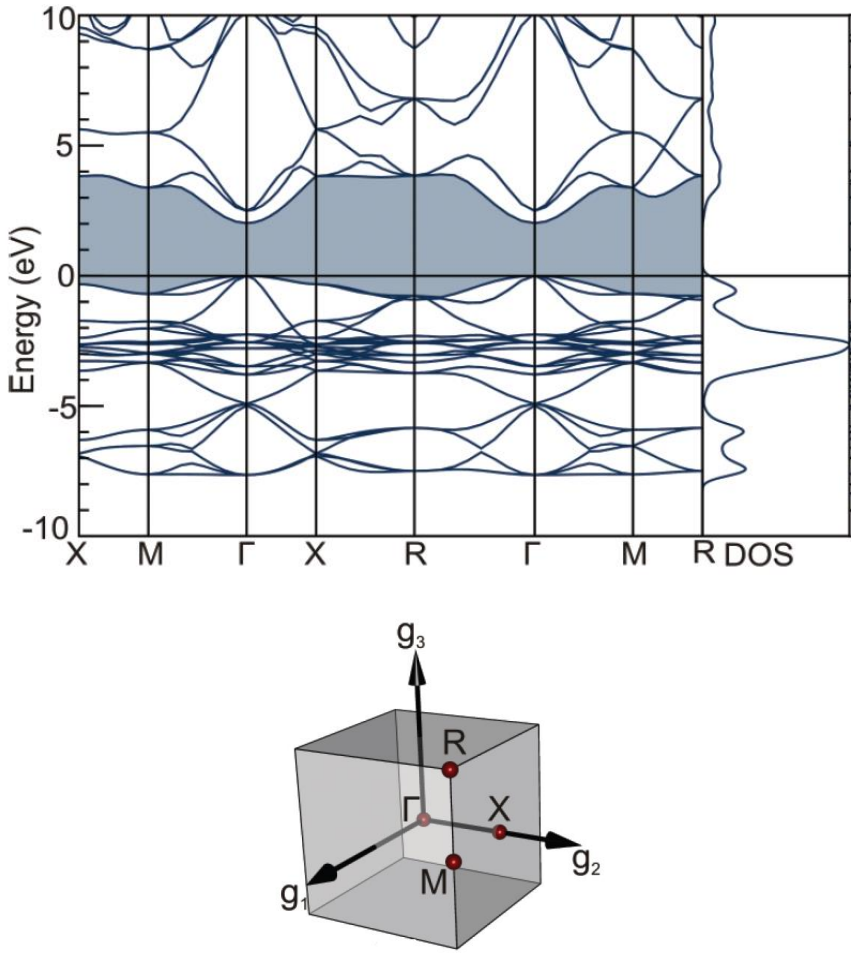

Figure 4.1 The band structure of Cu_2O and density of states from DFT calculations (above) and the associated Brillouin zones (below) [80]

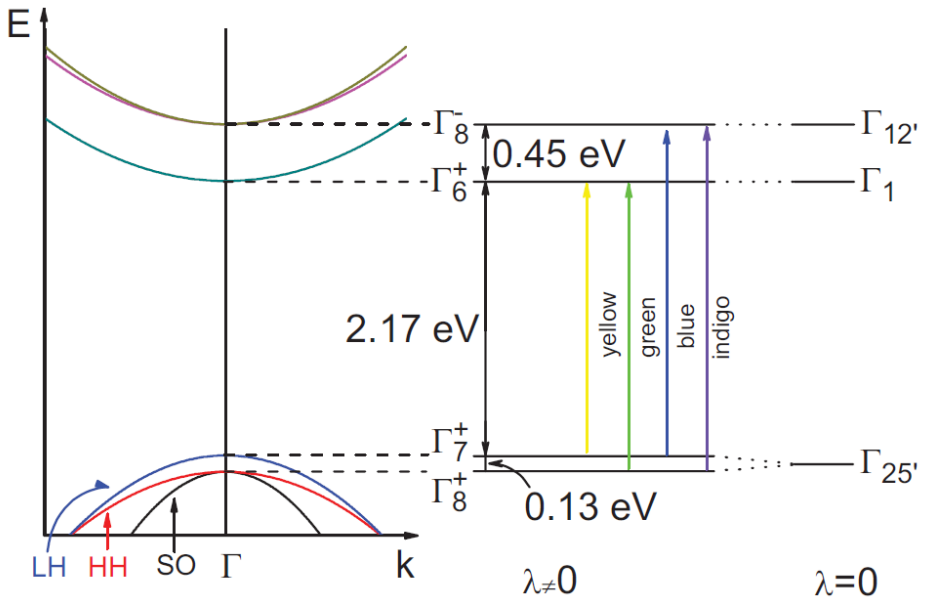

Figure 4.2 Energy-band diagram of Cu_2O around the Γ-point.[81]

4.2 Tauc Method

To determine the bandgap, the Tauc method was used. This method was developed by Tauc et al when exploring the optical properties of amorphous germanium. The method takes the optical absorbance and plots it against the energy to determine the bandgap. This method can be used to find the bandgap for any semiconductor material.[82]

The equation for determining the absorbance is shown in equation 7. In this equation α is the absorption coefficient, h is Planck's constant, ν is the photon's frequency, E_g is the bandgap, and A is the proportionality constant.

$$(\alpha h \nu)^{1/n} = A (h \nu - E_g) \quad (7)$$

The value of n represents the type of transition, either allowed or forbidden and either direct or indirect. The values for each of these scenarios is given in Table III.

Table III Possible transition types and the corresponding n values

Transition Type	n
Direct allowed	1/2
Direct forbidden	3/2
Indirect allowed	2
Indirect forbidden	3

To perform the Tauc analysis the first step is to obtain absorption data from a range of energies, both above and below the transition, then plot $(\alpha h \nu)^{1/n}$ versus $h \nu$. To determine the material's bandgap transition each n value is used and the plot resulting in a linear region stemming from or close to the x-axis most accurately describes the bandgap transition.

4.3 Cu_2O Data Collection

The first step to determining the bandgap of this work's Cu_2O film, was to get the absorption data from a Thermo Fisher Scientific Evolution 300 UV-Vis Spectrometer. The Cu_2O samples that were made for this data collection were made using the same process described in Chapter 2 and Chapter 3. Six samples were made with two substrates; FTO coated glass, and Au coated FTO coated glass, and at three different deposition times: 30 seconds, one minute, two minutes. The three sample thicknesses were explored to see how the thickness of the film might affect the bandgap. The one hour samples were not used for this part of the experiment because they were too thick to get reliable absorption data. The baseline correction used for the samples were either FTO coated glass for those samples deposited on FTO coated slides or Au/ FTO coated glass for the samples where Cu_2O was deposited on Au/ FTO coated glass.

Once the absorption data was obtained Tauc method was then employed. To calculate absorption coefficient (α) the following expression was used:

$$\alpha = 2.303A/L \quad (8)$$

Where A is the absorption and L is the thickness. The thickness was estimated using the Faraday's Law shown below as equations 9:

$$T = I * t * A * 10000/(n * F * \rho * S) \quad (9)$$

Where T is the thickness in μm, I is the current in Amps, t is the time in seconds, A is the atomic weight in grams/mol, n is the valence of the dissolved metal, F is Faraday's constant F = 96,485.309, ρ is the density in grams/cm^3, S is the deposition surface area in cm^2 and 10,000 is the constant to convert cm to μ.[83] This absorption coefficient was plugged into equation 7. This was then plotted versus h ν and the different n values were tested to determine the type of bandgap.

4.4 Results and Discussion

Using the Tauc plots the bandgap of the material can be extrapolated by taking the vertical section of the graph and continuing it down to intersect with the x-axis, and the energy value at the intercept is the bandgap. The bandgaps that were found using this method were fairly consistent for each of the samples including different thicknesses and from the FTO substrate sample to the Au/FTO sample. For the FTO/Cu_2O samples

shown in figure 4.3, the slope of this section, illistrated with a thick black line, intercepts the x-axis at about 2.6 eV for 30 second and one minute deposition times and 2.5 eV for two minute deposition time. For the FTO/Au/Cu_2O samples, shown in figure 4.4, the black line intercepts the x-axis at about 2.4 eV for one minutes, and 2.5 eV for two minute and 30 seconds.

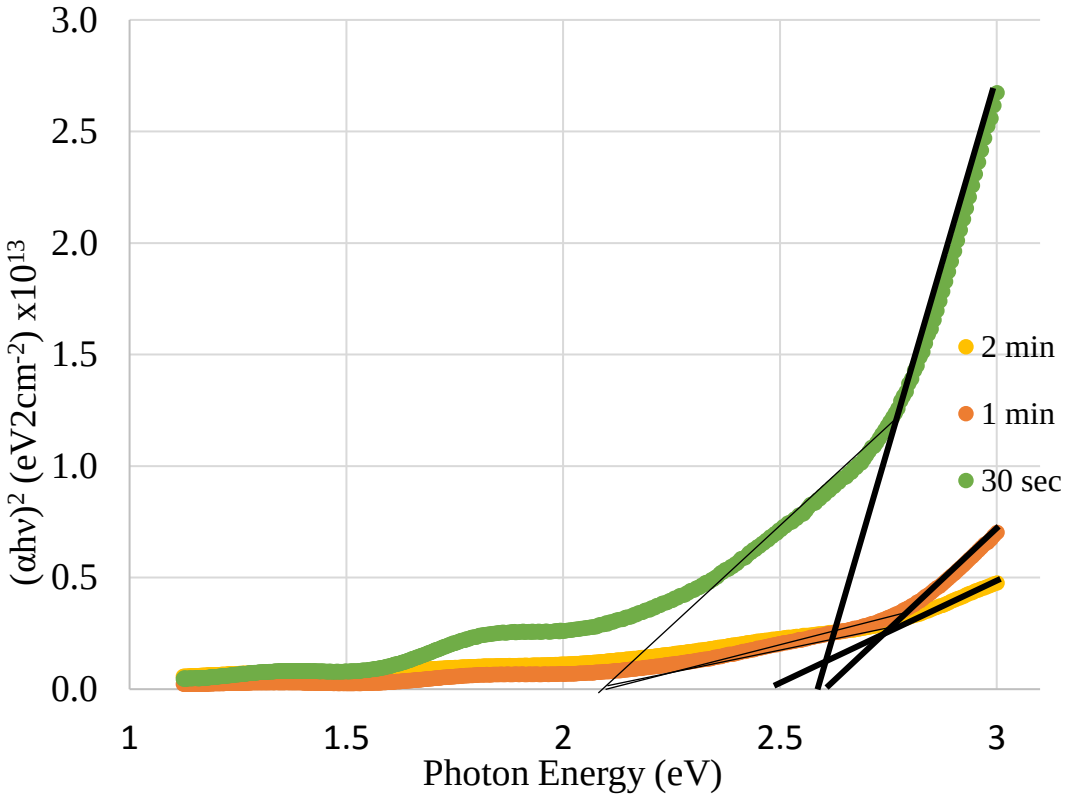

Figure 4.3 Tauc plot for the electrodeposited Cu_2O on FTO coated glass, for deposition times of 30 seconds, 1 minute, and 2 minutes.

The the Tauc plot slope for the one minute depostion of Cu_2O on Au/FTO sample was calculated to be about $1.1x10^{14}$. The slope value is related to the density of states, and the steeper the slope the flatter the band edge and the larger the effective electron mass. Gallium arsenide (GaAs) has a more shallow Tauc plot slope, calculated from a paper by Aspnes et al, to be about $4x10^{9}$.[84] Compared to Cu_2O the band edge is very steep

and the electron and hole effective mass is very low. ZnO was found to have a Tauc plot slope of $1x10^{12}$,[85] so the effective mass is larger than that of GaAs. The energy level of Cu_2O is shown in figure 4.1 to be relatively flat compared to GaAs and ZnO, and the comparison of the Tauc slopes for these materials confirms this comparison. Therefore, the effective electron mass for Cu_2O is large.

The Tauc plots showed that the films that resulted from the electrodeposition onto FTO and the films that resulted from the electrodeposition onto Au/FTO did have some differences in their absorption properties. The samples shown in figure 4.3 have an urbach tail that is the result of scattering of light from the surface of the material. In a standard Tauc plot there should be a sharp absorption edge where the plot goes from a flat line at zero absorption to a vertical line. The FTO/Au samples have a Tauc plot closer to the standard Tauc plot as shown in figure 4.4. The scattering on the Cu_2O/FTO samples is due to surface roughness. This roughness is apparent on the films when looking at it with the naked eye because the surface has a milky color to it. The SEM images in Chapter 2 show large faceted grains, these facets produce the scattering. The SEM images for the Cu_2O/Au films show much smaller grains that have smaller facets, so the scattering is less intense. One area that is unique for the Cu_2O/Au samples is the absorption hump at about 1.5 eV, this is believed to be due to the gold on the substrates.

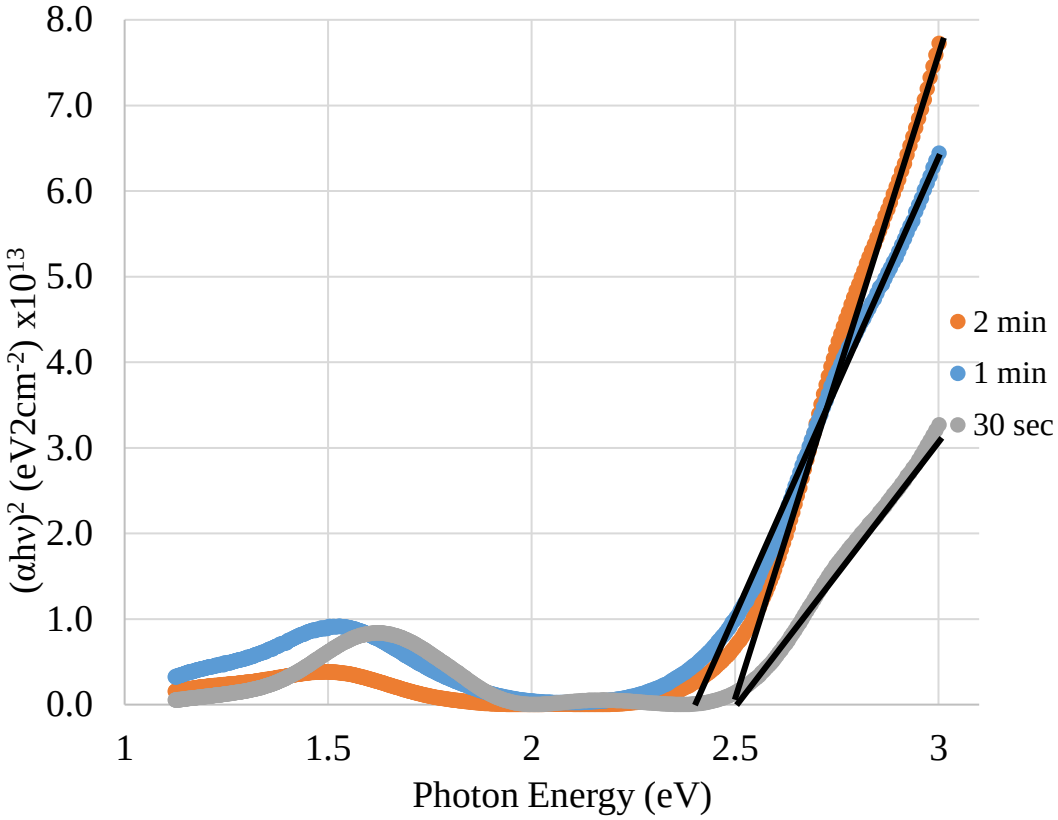

Figure 4.4 Tauc plot for the electrodeposited Cu_2O on gold coated FTO coated glass, for deposition times of 30 seconds, 1 minute, and 2 minutes.

Another theory as to why there is a tail for the FTO/Cu_2O samples is that there are two bandgaps represented by these Tauc plots. On the Tauc plot for the two-minute deposition for the FTO/Cu_2O there are two distinct flat sections. Based on the band structure information in section 4.1.1 there are two gaps to consider, the first is the optical bandgap, which has a width of about 2.6 eV. This is the bandgap that is represented in each of the Tauc plots. The second gap is also direct but the transition is forbidden[80,81] and has a width of 2.17eV. This gap is only shown in the Tauc plots from the FTO/Cu_2O samples. The line drawn for the absorption edge, identified using a thinner black line on figure 4.3, intercepts the x-axis at about 2.1 eV. The Au/FTO films

do not show the second bandgap at 2.1 eV and that is because this film is more n-type than the Cu_2O film on FTO. An n-type semiconductor has more electrons in the conduction band that means, in this case, the conduction of electrons will only take place in the wider of the two bands.

Based on the findings from the Tauc plot, the bandgap of electrodeposited Cu_2O on FTO coated glass is too wide for the purposes of a tandem device. However, there is a decrease in the bandgap under the influence of gold, which also resulted in the better Tauc plot showing limited amounts of scattering.

CHAPTER 5

5. n-Type Cu_2O

5.1 Background of n-Type Cu_2O

Cuprous oxide is intrinsically a p-type material meaning that holes are the primary carrier and electrons are the secondary carrier. One of the goals of this research was to look into the fabrication of n-type Cu_2O that can be used in the formation of a homojunction solar cell. The existence of an n-type Cu_2O has been discussed and could be the result of oxygen vacancies.[41,49] There has also been work that shows that n-type Cu_2O can be formed by doping the film with excess copper. This doping is accomplished through thermal diffusion. The idea is that this dopant of Cu ions will remove Cu vacancies and introduce Cu interstitials and Cu on O sites, changing the material from a p-type to an n-type.[19,86]

Han, et al worked on homojunction Cu_2O solar cells, where the deposition was carried out with two different pH levels, below 8.0 and above 9.0 for n-type Cu_2O and p-type Cu_2O respectively.[19,86] Other works reported the effect that pH has on controlling the carrier type for Cu_2O, where the pH of the electrolyte was brought down to 4.9 for electrodeposition of n-type Cu_2O.[18,44,86] It was reported by Scanlon and Watson that intrinsic n-type defects in Cu_2O do not result in n-type behavior.[40] This research focused on the work from Fernando, et al. Their group boiled copper plates in a copper sulfate to convert the Cu to n-type Cu_2O.[42] The results from this paper show an n-type Cu_2O. The goal here was to follow this research to determine if n-type Cu_2O

could be obtained using this method. The substrate was modified to see if the result would yield an n-type Cu_2O film that could be used in a homojunction solar cell and part of a tandem solar cell. The modifications consisted of using deposited copper on glass and then converting it to Cu_2O instead of converting a copper plate. This was to allow for a solar cell that light could be transmitted through if it is not absorbed.

5.2 Experimental Reagents

All chemicals that were used for this work were as follows: (i) copper (II) sulfate pentahydrate, greater than 98.0% purity, purchased from Sigma Aldrich (ii) sulfuric acid 95-98% pure, purchased from Sigma Aldrich; (iii) acetone, ACS grade, purchased from Fisher Scientific.

5.3 Substrate Preparation

Three different types of samples were explored for the conversion of Cu to Cu_2O. The first substrate is the most common for the boil method, a solid piece of Cu, in this case a thin Cu sheet was used. The next substrate that was used was electrodeposited Cu onto FTO coated glass. The final substrate was sputtered Cu onto either glass or FTO coated glass.

5.3.1 Copper Sheet

The first step was to duplicate the experimental procedure from Fernando, et al by converting copper metal to Cu_2O. A thin copper sheet was used as the substrate. This

sheet was 71nm thick and was cut down to a 2 by 5 cm sheet. The copper sheet was then cleaned in an ultrasonicator three times using 2 vol % Micro-90 in DI water, DI water, and finally acetone.

5.3.2 **Electrodeposition of Copper**

Electrodeposition of copper was also explored because a glass substrate, which is ideal for the tandem solar architecture, could be used. A rectangular piece of FTO coated glass was cleaned using the same procedure described above. Once cleaned the substrate was attached in a two electrode system with a platinum counter electrode. Both of these electrodes were submerged in the electrolyte and connected to a voltage source. The electrolyte was a 0.05 M copper (II) sulfate pentahydrate in DI water. The solution was brought to a pH between one and three using sulfuric acid. This deposition was run for one minute at five volts.

5.3.3 **Sputter Coating of Copper**

Another method that was used to deposit the copper was sputter coating. The substrate for this method was a thin glass slide or FTO coated glass, and both were cleaned prior to the deposition using the same method described in section 5.2.1. For this method the coater that was used for the gold deposition from Chapter 3 was used but the gold target was replaced by a copper target (99.99% 57mm dia x 0.1mm thick, from EMS) a number of different thicknesses were deposited (20, 30, 50, 85, 125nm).

5.4 Conversion from Cu to Cu_2O

The next step of this experimental procedure was to take each of the three types of thin films of copper and convert it to Cu_2O. The substrates were clipped to Teflon covered alligator clips that were attached to copper wire. The wire was then draped over the edge of a beaker and submerged into a boiling solution of 10^{-3} M copper sulfate pentahydrate in DI water. The substrate was left in the solution for one hour. During this hour if the solution level dropped the water was replaced.[42] After an hour the film was rinsed with DI water. Each of the substrates were boiled in individual beakers.

5.5 Characterization

The films of Cu_2O were characterized to determine whether they were n-type or p-type by performing a hot probe test and a solar simulation with the p-type electrodeposited Cu_2O. Next they were analyzed using SEM to compare the growth of the three different films. Finally, XRD was used to determine if the copper had convert to Cu_2O completely and what if any other phases were present.

5.5.1 Hot Probe Test

One way to determine if the deposited film resulted in n-type is a hot probe test. This test was performed using a multi-meter set to read the current. The pins of the multi-meter were set on the surface of the film one centimeter apart, one of the pins was heated and the current was observed. If the positive pin is heated and the current reads positive then the film is n-type, and if it reads negative then the film is p-type.

5.5.2 **Solar Simulation**

A Newport model solar simulator was used to determine if the p-type and n-type Cu_2O would work in as solar cell. The n-type process that was used for this testing was the sputtered copper because it was the most consistent film. To perform this test three samples were made: the first was n-type Cu_2O deposited onto FTO followed by electrodeposited p-type Cu_2O, next was electrodeposited Cu_2O deposited onto FTO followed by the n-type Cu_2O, and last was electrodeposited Cu_2O deposited onto Au and FTO followed by n-type Cu_2O. All three devices had a back contact of 60nm thick Au. The simulation was completed using from -1 to 1 volts.

5.5.3 **SEM**

Scanning electron microscopy was used to understand the conversion of the copper to Cu_2O. First images were taken of the copper sheet and the sheet after boiling. This comparison is shown in figure 5.1 and 5.2. Next the images of electrodeposited copper boiled in the copper sulfate were taken using the SEM, this is shown in figure 5.3. The final image was taken of the sputtered copper converted to Cu_2O in figure 5.4.

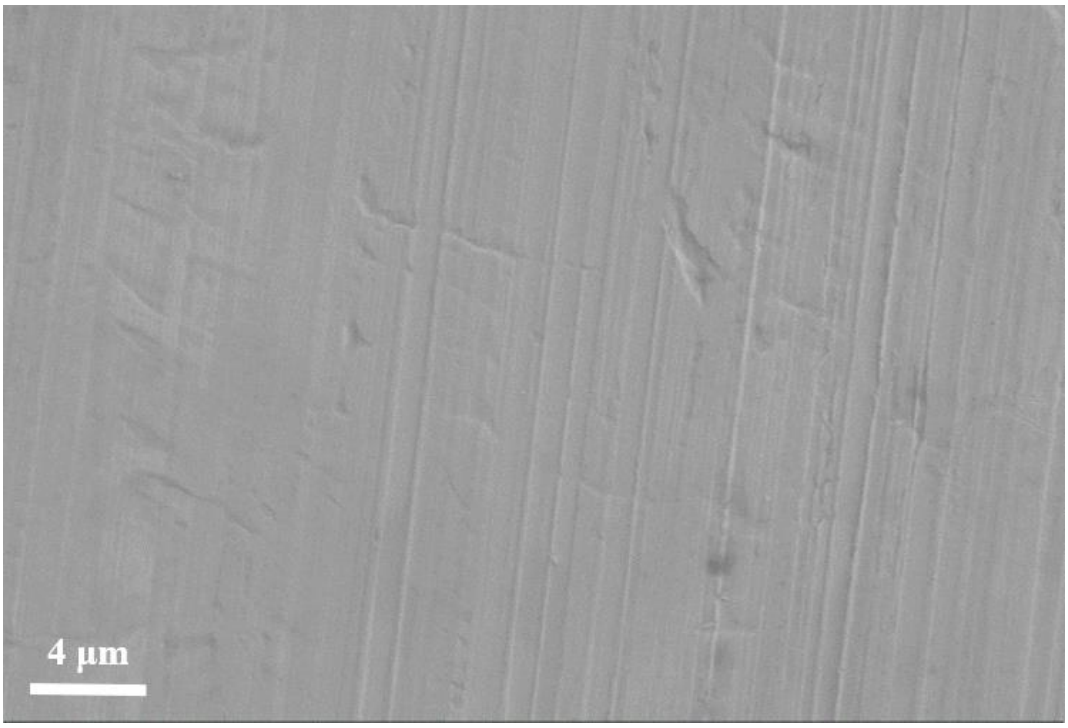

Figure 5.1 SEM image of a copper sheet

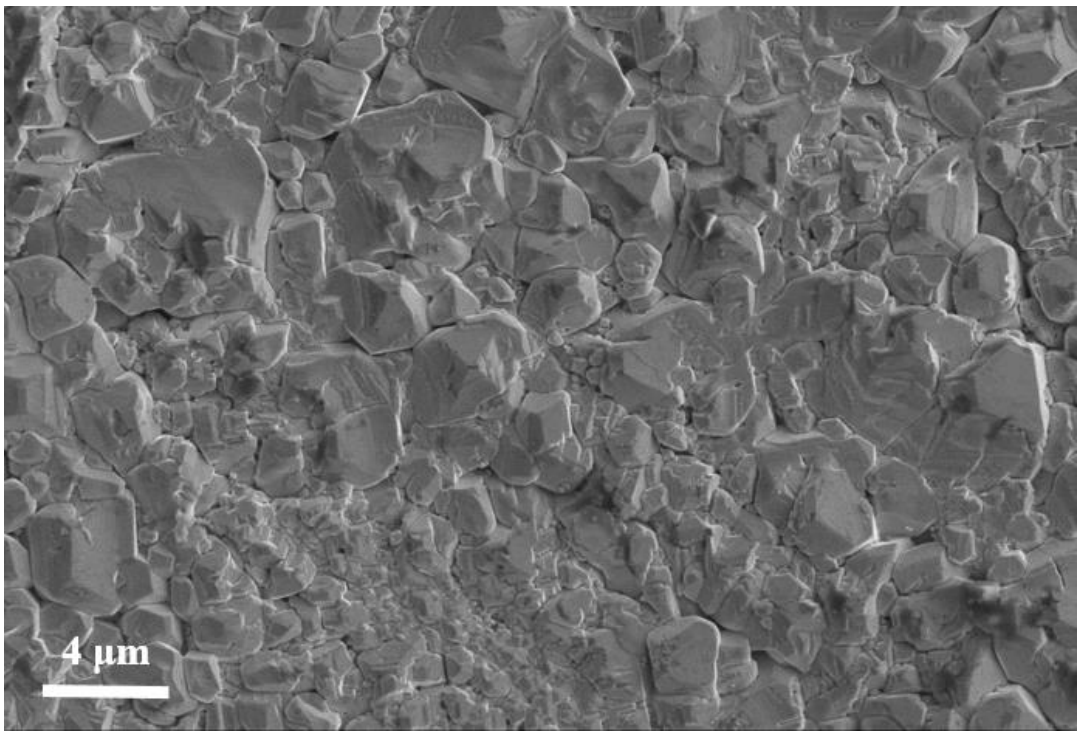

Figure 5.2 SEM image of a copper sheet that has been boiled in copper sulfate to convert it to Cu_2O

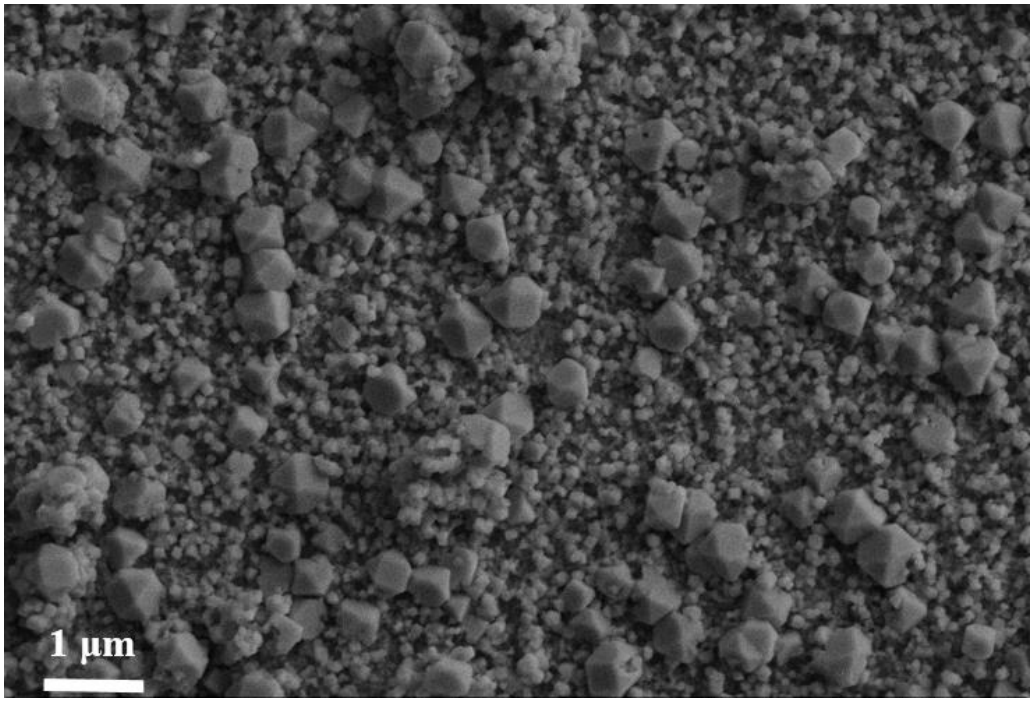

Figure 5.3 SEM image of electrodeposited copper on FTO coated glass that has been converted to Cu_2O by boiling in copper sulfate.

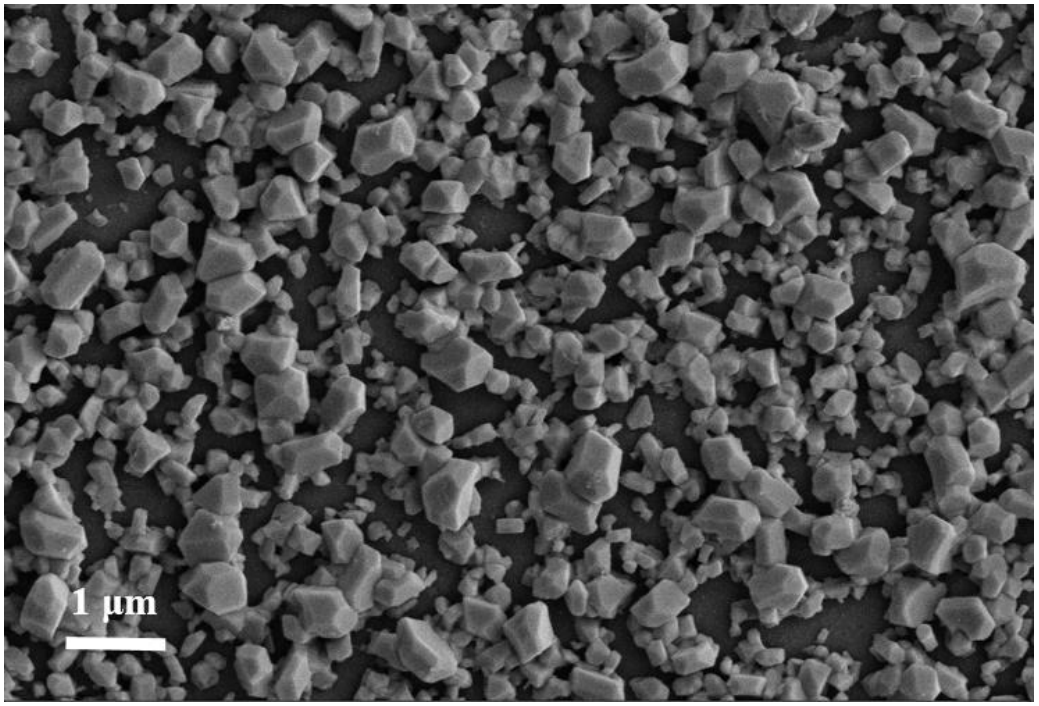

Figure 5.4 SEM image of sputtered copper on glass that has been converted to Cu_2O by boiling in copper sulfate.

5.5.4 **XRD**

X-ray diffraction was used to determine phases of copper oxide that are present, and how much, if any, copper remained from the boiling process. All three types of substrates were analyzed using an X'Pert PANalytic XRD. The first is shown in figure 5.5, showing the pattern resulting from the boiled copper sheet. The next pattern, figure 5.6, shows the results from the electrodeposited copper on FTO coated. The final pattern, figure 5.7, is for the sputter coated copper on glass.

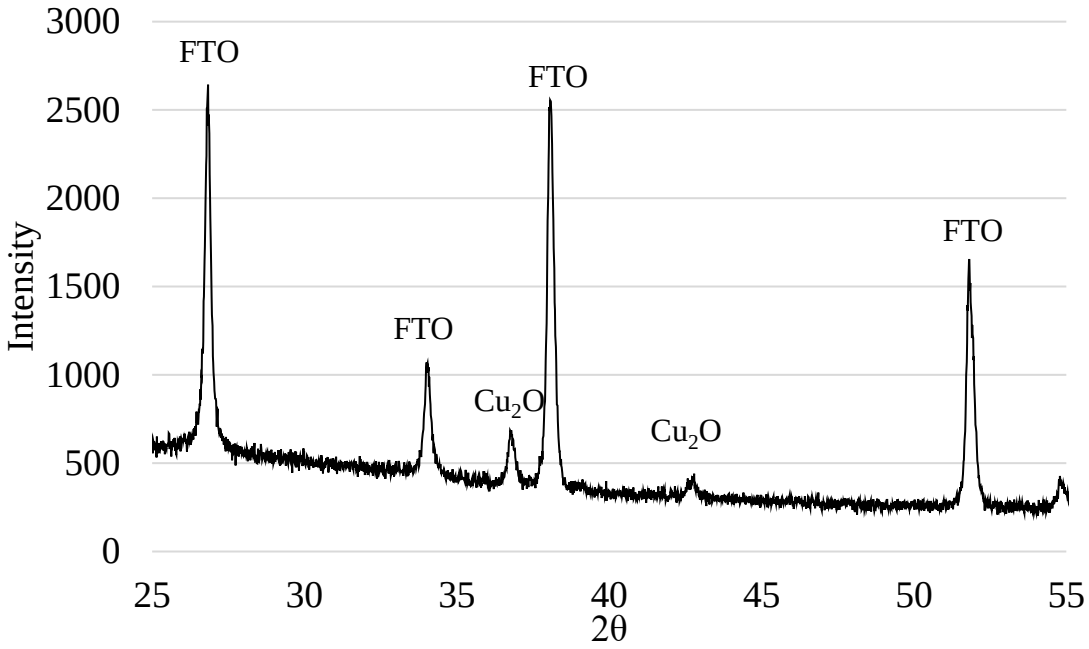

Figure 5.5 XRD data of Cu_2O resulting from a copper sheet boiled in copper sulfate.

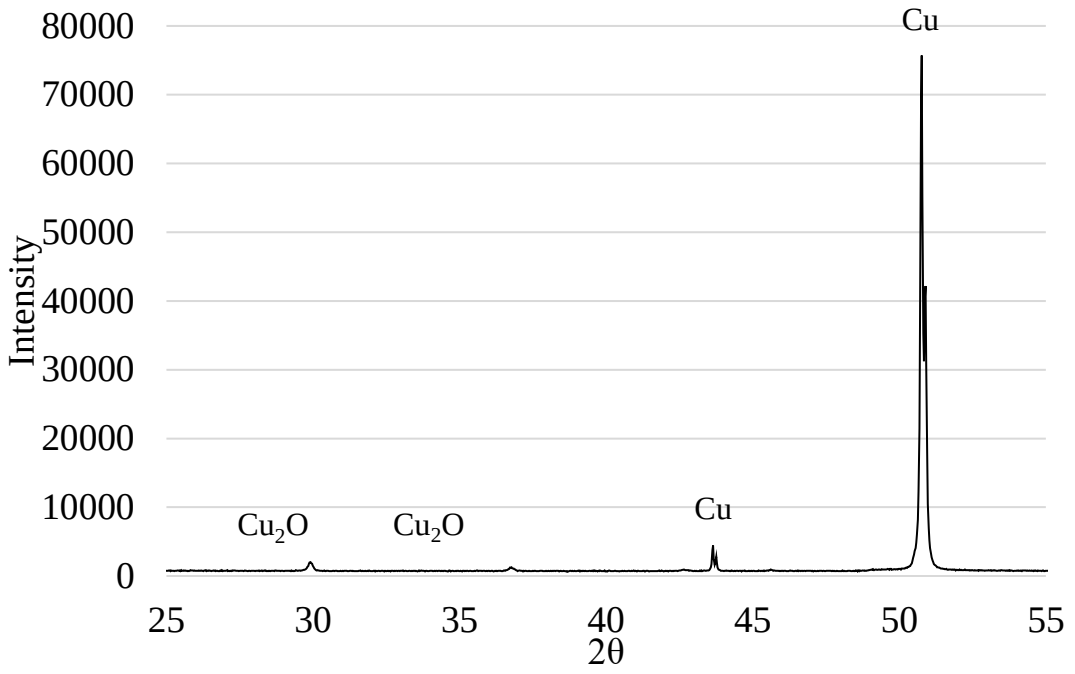

Figure 5.6 XRD data of Cu_2O resulting from electrodeposited copper onto FTO coated glass and then boiled in copper sulfate.

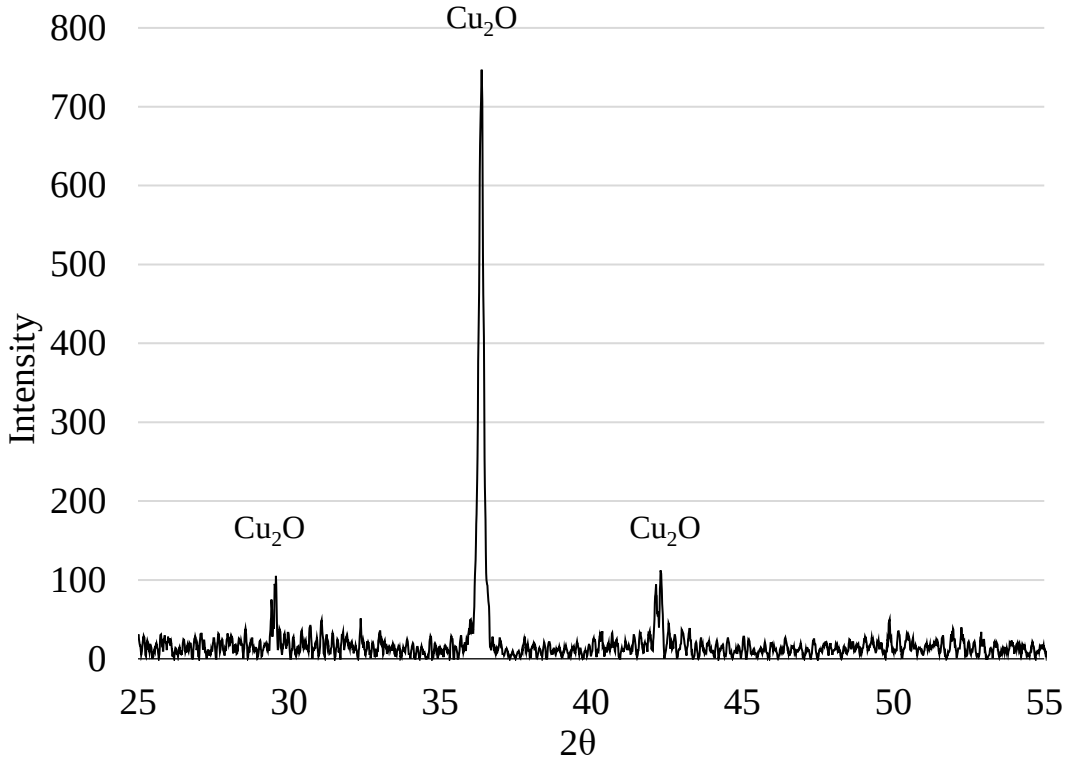

Figure 5.7 XRD data of Cu_2O resulting from a sputtered copper onto glass and then boiled in copper sulfate.

5.6 Results and Discussion

The boiled copper sheet method resulted in a film that was flaking and uneven. In XRD the results were inconclusive. Since the substrate is copper it was impossible to determine using this technique if the top layer was 100% Cu_2O, though there was conversion of the copper to Cu_2O it is unclear from the XRD results if the top layer of material contained any copper along with the Cu_2O. The SEM results showed a growth of distinct grains compared to the SEM image from figure 5.1, which showed the copper sheet before boiling.

The electrodeposition resulted in even films that were consistent in their replicability. The one issue that arose was if the copper film was exposed to air for any length of time after the electrodeposition and before boiling, then the film would oxidize unevenly and result in a flaking and uneven Cu_2O film after boiling. The XRD results showed that there was full conversion from Cu to Cu_2O.

Initially a glass microscope slide was used for the sputter coated films. These were inconsistent. The best film resulted from the 125nm thick sputtered copper, the thinner samples flaked off during the boiling process. The second attempt used FTO coated glass, which resulted in a much more even and stable film. The XRD results from the sputter coated sample show similar results to the electrodeposited Cu.

The hot probe test was inconclusive, the multimeter would swing from positive to negative. The solar simulation results did not show any photovoltaic or photocurrent response, though this could have been due to the quality of the films that were grown. The sputtered copper film converted to Cu_2O but did not fully cover the surface, so there could have been pin holes or the p-type and n-type materials might not have made

enough of a connection to form the p-n junction. From these results it can be assumed that the n-type characteristics that were presented from the paper by Fernando et al were not reproduced for this work..

CHAPTER 6

6. Conclusions

This research is fueled by the idea that there are alternative energies such as solar that have only just begun to be tapped into and are needed in order to alleviate the use of destructive and limited energy source such as fossil fuels. The work to make photovoltaic technologies cheaper and more efficient is the key to obtaining a larger market. The biggest problem with efficiency is that energy loss is inevitable because of the solar spectrum. There will always be losses, particularly with single junction solar cells, because there is energy lost when a photon exceeds the bandgap and the photons that have a lower energy than the band gap are not absorbed. Silicon has the best efficiency for a single junction solar cell because it has a bandgap of 1.1 eV this bandgap width balances the described losses, and therefore, silicon solar cells are dominating the market at 21% efficient. Energy losses can be further minimized by stacking solar cells so that more photons are absorbed. The use of silicon solar cells as the bottom layer of this stack is a promising path to take. The overarching goal of this research was to establish a wide band gap solar cell that could be used as the top cell of a tandem solar cell. This top cell would have to be cheap and grown on the glass that encases the top layer of the single junction silicon solar cell. Cu_2O was the focus for this work as the wide band gap absorber layer for the wide bandgap solar cell that can be used in a tandem solar cell.

Electrodeposition was identified as the preferred process for the deposition of Cu_2O because it is a low cost process and results in even films that can be scaled to manufacturing sizes. Two different electrolytes were explored. The two types were each deposited using a two electrode system onto FTO coated glass and the grain growth was explored by depositing the film for times from 30 seconds to one hour. The SEM images showed that E1 resulted in a growth that was not well defined at one hour, E2 resulted in grains that were a flowering dendritic shape. The XRD results showed that both films were Cu_2O but that there was a small amount of Cu present in each film.

The ideal grain shape for a thin film solar cell would be a columnar shape so that the electrons can flow through the grain without interruption of grain boundaries, where recombination of the electron and hole is common. The next step was to take the two different films deposited for one hour and manipulate the growth so that the grain shape was closer to the ideal columnar shape. This was achieved using the well-known relationship between Cu_2O and Au, and using the Au as a seed to grow the Cu_2O. The Au seed layer was deposited using a sputter coater, depositing a thin layer of Au, and then baking the film to turn the thin film of Au into Au nano-islands on FTO coated glass. This layering of Au nano-islands on FTO coated glass was then used as the working electrode for the electrodeposition. The SEM results showed smaller grains and that grain growth was much more controlled and the grains were densely packed. The grains also showed a strong faceting. XRD showed that with the presence of Au nano-islands, the copper that was growing with E2 was no longer present, but the copper was still present for the E1 sample even with Au nano-islands. TEM images from a sample that was cut out of the E2 sample on Au/FTO, showed that the Cu_2O that was growing

on the Au was growing epitaxially, confirming that there is an orientation relationship between the two layers. Finally, the E2 films grown on Au/FTO and FTO were subject to electrical characterization and although photovoltaic properties were not present there was an indication of photocurrent properties in the film grown on Au/FTO. This was because the Cu_2O grown on Au/FTO was more resistant compared to the film grown on FTO, and therefore the photoconductivity was more obvious.

The optical properties for E2 on Au/FTO and FTO were explored due to the importance of the bandgap estimation for this work and the lack in consistency in the reported bandgap for Cu_2O in the literature. The optical measurement was completed using UV/Vis spectrometer to get the absorption data for three samples from each substrate. Each sample had a different deposition time (30 seconds, one minute, and two minutes). Using the Tauc method a Tauc plot was developed using the absorption data and an estimation of the film thickness. This Tauc plot showed that the bandgap for Cu_2O is direct and allowed. Using the absorption edge the bandgap was found to be around 2.6 eV for the FTO substrate sample and 2.5 eV for the Au/FTO substrate sample. The two Tauc plots showed some significant differences. In the Au substrate sample, the Tauc plot had an absorption edge that was very close to the x-axis unlike the FTO substrate sample, which had a large tail before the absorption edge. This tail could be a result of the scattering of light on the surface of the film, but there also appears to be a second straight section just before the large absorption edge at 2.6 eV, which intersects the x-axis at about 2.1 eV. Based on the literature there are two bandgaps for Cu_2O one at 2.64 eV and one at 2.17 eV, these two gaps can only be seen in the Tauc plot for the sample deposited on FTO. The other area of difference comes from the Tauc

plot for the Au/FTO sample, there is a hump at 1.5 eV, which is believed to be from the Au that is present in the film. The results of this measurement showed that the Au/FTO films had less scattering and band gap around 2.5 eV while the FTO samples potentially had two bandgaps one at 2.6 eV and the second at 2.1 eV.

The development of n-type Cu_2O has been an area of interest for a homojunction solar cell with p-type Cu_2O. This is due to the idea that a homojunction solar cell has the potential for a higher efficiency compared to a heterojunction solar cell. The method for obtaining an n-type Cu_2O for this research was from the work of Fernando et al.[42] The goal of this chapter was to establish if this work was reproducible and could be manipulated for use in the application being explored. The paper uses a copper plate and boils it in a copper sulfate solution, this process was duplicated using a copper sheet. This substrate is not ideal because the back and front contact have to be transparent for use in a tandem cell, it was also difficult to determine if the film that was made was 100% Cu_2O because there was always going to be copper present from the substrate. The modification that was explored was depositing copper onto FTO and boiling this thin film of Cu to transform it into Cu_2O. This was completed first by electrodepositing Cu onto FTO. The resulting Cu_2O film was evenly coated but it scratched off easily. Another problem with this film was that the electrodeposited Cu was not stable before boiling, if left in air for only a couple of minutes the film would change color, become flakey and would flake off into the boiling solution. The next deposition process of Cu that was explored was sputter coating. Using a copper target, the FTO coated glass was coated with 125nm thick layer and then boiled. This process resulted in the most reliable film, it also scratched off easily but it did not flake into the solution. The XRD results

showed that each of these processes produced Cu_2O and Cu was not present except in the case where it was expected. The SEM results showed similar growth of Cu_2O for the electrodeposited and the sputter coated samples with slightly larger grains from the sputter coated sample. The boiled copper sheet resulted in large grains of Cu_2O. The sputter coated sample was the most reliable of the three samples and would allow the deposition of Cu_2O onto an insulating surface as well as a conduction surface, which will allow for further testing. The hot probe test was inconclusive so the carrier type was not verified using this method. A solar cell was attempted using the electrodeposited p-type from Chapters 2 and 3. Three solar cells were tested, FTO/n-type/p-type/Au, FTO/p-type/n-type/Au, and FTO/Au/p-type/n-type/Au. This testing showed no photovoltaic or photocurrent responses for any of the attempted devices.

CHAPTER 7

7. Future Work

The research completed for this thesis is just the tip of the iceberg for Cu_2O thin film fabrication and photovoltaic work. While the results that have come from this thesis are interesting and insightful, it seems to indicate that Cu_2O would not make for an ideal material for the absorber layer of the top cell of a tandem device. There are some areas of work that could be explored to improve upon these films for use in other applications.

7.1 p-Type Cu_2O

In Chapters 2 and 3 the deposition process for Cu_2O is described, along with how the film microstructure was modified. This resulted in a more controlled film that was fully densified. One area that would be interesting to delve into would be to change the carrier concentration of the film. This would allow for manipulation of the depletion region of the p-n junction. The carrier concentration was not determined or determinable for these films because they were deposited onto a conductive substrate. One method that would allow for carrier concentration testing would be the Cu_2O film that resulted from the sputtering of copper onto glass. The problem with the film developed by that method for this research was that the film did not fully cover the glass after conversion so it would require multiple layers of deposition.

From the attempted solar cells using FTO as the substrate and the n-type material, it was determined that the Cu_2O that was deposited onto Au/FTO had a photoconductivity response. The current was very low, but it was shown from the work

by Du Pasquier et al, that the small photocurrent can be found for the photon energies where absorption occurs for a material.[87] The set up for this characterization technique is shown in figure 7.1.

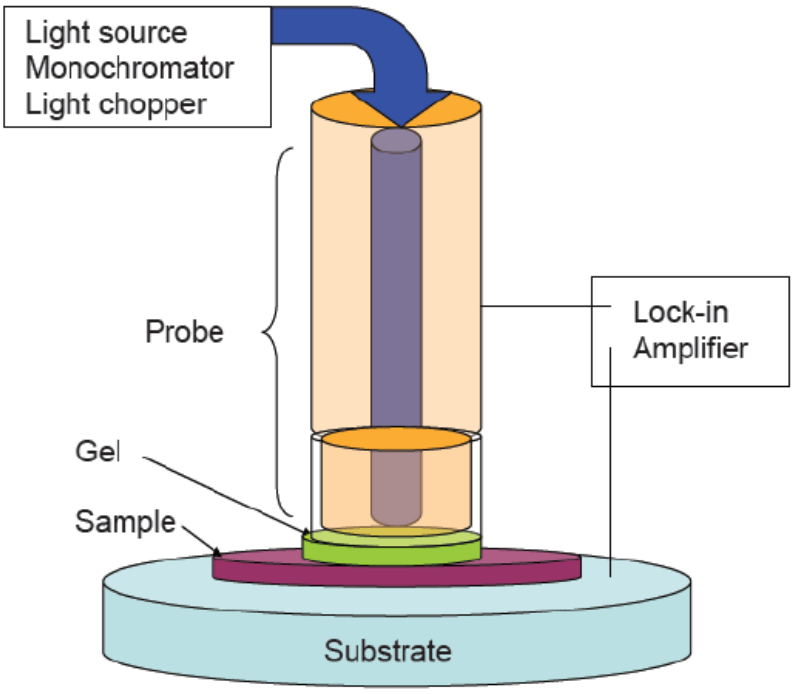

Figure 7.1 Set up for photocurrent measurements[87]

The wavelength is picked through the monochromator where a fiber optic refection probe is attached. The probe has a metal casing and it is electrically connected to the sample's surface with a gel electrolyte. A lock-in amplifier is required because the signal is so low. The amplifier is attached to the metal casing of the probe and the substrate contact that the sample is deposited on. This experiment will allow for photocurrent measurements from the photon energies that are associated with the absorption that was determined in Chapter 4.

7.2 n-Type Cu_2O

In Chapter 5 it was determined that the Cu_2O film that resulted from the boiling method was not an n-type semiconductor. The carrier type was first tested with the hot probe method but this was inconclusive, so the next step was to take the presumptive n-type material and pair it with the p-type that was being grown using electrodeposition described in Chapters 2 and 3. This test resulted in a film that did not show photovoltaic properties or photocurrent properties. This leads to the belief that what was made by boiling copper in copper sulfate did not lead to n-type Cu_2O. The first step for confirming this finding would be to increase the coverage of the Cu_2O from boiled sputtered Cu, this could be completed by repeating the sputtering and boiling once or twice more. Another possible way of modifying this n-type material would be to use a dopant in the boiling solution. This could result in a more reliable n-type Cu_2O. There is work indicating that Cu, fluorine (F), chlorine (Cl), and bromine (Br) might make for stable dopants in Cu_2O and that the doping of these elements would result in n-type Cu_2O.[19,45]

7.3 Solar Cell Fabrication

The solar cells that were created during the research of this process did not result in any photovoltaic properties. There are quite a few paths that can be taken to improve these results described in Chapter 3 and 5. The first would be to understand the p-type material, Chapter 3 described research where the p-type Cu_2O was tested on FTO to determine if this p-n junction would result in a solar cell and the results indicated that it would not. One concern for this is that the unmodified Cu_2O on FTO grew as a film with

gaps between the grains, this could be mitigated by growing a thicker film. The growth is limited by the resistivity of the film as it grows thicker, so when the surface of the Cu_2O is no longer the optimum area of growth, the growth should continue in the gaps between the grains.

The modified Cu_2O grown on Au/FTO might not have made a good enough p-n junction because the interference with the gold between the two layers. Therefore another area that could be further explored is the use of a well-established n-type material that has been successfully paired with Cu_2O, such as ZnO. Over the years ZnO has been researched frequently as the n-type in Cu_2O heterojunction solar cell, with mixed results.[23,29,30,32-35,66,79] This would require a well-known deposition process for ZnO so that the only variable factor would be the Cu_2O, the effect of the thickness of the film and the effect of the gold on electrical properties of the solar cell.

BIBLIOGRAPHY

[1] R. F. Service. Is It Time To Shoot For The Sun? *Science.* 309, 2005, 548-551.

[2] J. Potocnik. Renewable Energy Sources and the Realities of Setting an Energy Agenda, *Science.* 315, 2007, 810-811.

[3] T. Conti, P. Holtberg, J. A. Beamon, S. Napolitano, A. M. Schaal, J. T. Turnure, and L. Westfall. *International Energy Outlook 2013* U. S. Energy Information Administration, DOE/EIA-0484, 2013.

[4] "International Energy Statistics." 2013.Web. <http://www.eia.gov/cfapps/ipdbproject/IEDIndex3.cfm?tid=2&pid=2&aid=12>.

[5] J. L. Sawin, C. Lins, E. Musolino, K. Petrichenko, W. Rickerson, K. Seyboth, J. Skeen, B. Sovacool, F. Sverrisson, and L. E. Williamson. *Renewables 2015 Global Status Report* REN21, 2015.

[6] Q. Schiermeier, J. Tollefson, T. Scully, A. Witze, and O. Morton. Energy Alternatives: Electricity without Carbon, *Nature.* 454, 2008, 816.

[7] M. Rekinger, F. Thies, G. Masson, and S. Orlandi. *Global Market Outlook for Solar Power 2015-2019* Solar Power Europe, 2015.

[8] "Research Cell Efficiency Records." 02-25-2016 2016.Web. <http://www.nrel.gov/ncpv/>.

[9] S. P. Philipps, A. W. Bett, K. Horowitz, and S. Kurtz. *Current Status of Concentrator Photovoltaic Technology* Fraunhofer ISE/NREL, CPV Report 1.2, 2016.

[10] V. Vijayakumar, and D. P. Birnie. Optical and Electronic Simulation of Gallium Arsenide/Silicon Tandem Four Terminal Solar Cells, *Solar Energy.* 97, 2013, 85-92.

[11] C. H. Seager. Grain Boundary Recombination: Theory and Experiment, *Journal of Applied Physics. 6* 52, 1981, 3960.

[12] "CdTe Photovoltaic Cell Graphic." 2013.Web. <http://www.nrel.gov/pv/images/graphic_cdte_cell.jpg>.

[13] C. H. Henry. Limiting Efficiencies of Ideal Single and Multiple Energy Gap Terrestrial Solar Cells, *Journal of Applied Physics.* 51, 1980, 4494-4500.

[14] "Photovoltaic Cell Structure Basics." 08-19-2013 2013.Web. <http://energy.gov/eere/energybasics/articles/photovoltaic-cell-structure-basics>.

[15] L. Fraas, and L. Partain. *Solar Cells and their Applications*. 2nd ed. Hoboken, NJ: John Wiley & Sons Inc., 2010. Print. Wiley Series in Microwave and Optical Engineering .

[16] D. Trivich. Photovoltaic Cells and Their Possible Use as Power Converters for Solar Energy, *Ohio Journal of Science. 5* 53, 1953, 300-314.

[17] L. C. Olsen, F. W. Addis, and W. Miller. Experimental and Theoretical Studies of Cu_2O Solar Cells, *Solar Cells.* 7, 1982, 247-279.

[18] C. M. McShane, and K. Choi. Photocurrent Enhancement of n-Type Cu_2O Electrodes Achieved by Controlling Dendritic Branching Growth, *Journal of the American Chemical Society.* 131, 2008, 2561-2569.

[19] K. Han, and M. Toa. Cu Diffusion Doping in Electrodeposition n-Type Cu_2O, *216th ECS Meeting.* Abstract #760, 2009, .

[20] N. Gupta, S. Rajandra, F. Wu, J. Narayan, C. McMillen, K. F. Poole, G. F. Alapatt, D. Sulejmanovic, S. Hwu, M. Young, G. Teeter, and H. S. Ullal. Deposition and Characterization of Nanostructured Cu_2O Thin-Film for Potential Photovoltaic Applications, *Journal of Materials Research. 13* 28, 2013, 1740-1746.

[21] M. Li, W. Wu, K. Liu, G. Hu, and H. Xu. Three-Dimensional Assembly and Electrical Properties of Cu_2O/ZnO Heterojunction via an Electrochemical Superfilling Method, *Electrochimica Acta.* 71, 2012, 100-105.

[22] L. Chen. Review of Preparation and Optoelectronic Characteristics of Cu_2O-based Solar Cells with Nanostructure, *Materials Science in Semiconductor Processing. 5* 16, 2013, 1172-1185.

[23] T. Minami, T. Miyata, and Y. Nishi. Cu_2O-based Heterojunction Solar Cells with an Al-doped ZnO/Oxide Semiconductor/Thermally Oxidized Cu_2O Sheet Structure, *Solar Energy.* 105, 2014, 206-217.

[24] T. Minami, Y. Nishi, and T. Miyata. Efficiency Enhancement Using a $Zn_{1-x}Ge_x$-O Thin Film as an n-Type Window Layer in Cu_2O-Based Heterojunciton Solar Cells, *Applied Physics Express.* 9, 2016, 052301.

[25] T. Minami, Y. Nishi, and T. Miyata. Heterojunction Solar Cell with 6% Efficiency Based on an n-Type Aluminum-Gallium-Oxide Thin Film an p-Type Sodium-Doped Cu_2O, *Applied Physics Express.* 8, 2015, 022301.

[26] R. J. Iwanowski, and D. Trivich. The Influence of Hydrogen Ion Bombardment on the Photovoltaic properties of Cu/Cu_2O Schottky Barrier Solar Cells, *Radiation Effects Letters.* 76, 1983, 87-92.

[27] J. Katayama, K. Ito, M. Matsuoka, and J. Tamaki. Performance of Cu_2O/ZnO Solar Cell Prepared by Two-Step Electrodeposition, *Journal of Applied Electrochemistry.* 34, 2004, 687-692.

[28] M. Deo, S. Mujawar, O. Game, A. Yengantiwar, A. Banpurkar, S. Kulkarni, J. Jog, and S. Ogale. Strong Photo-Response in a Flip-Chip Nanowire p-Cu_2O/n-ZnO Junction, *Nanoscale.* 3, 2011, 4706-4712.

[29] M. Deo, D. Shinde, A. Yengantiwar, J. Jog, B. Hannoyer, X. Sauvage, M. More, and S. Ogale. Cu_2O/ZnO Hetero-Nanobrush: Hierarchical Assembly, Field Emission and Photocatalytic Properties, *Journal of Materials Chemistry.* 22, 2012, 17055-17062.

[30] M. Zemzemi, and S. Alaya. Band Offset of the ZnO/Cu_2O Heterojunction from ab Initio Calculations, *Superlattices and Microstructures.* 64, 2013, 311-318.

[31] T. Minami, H. Tanaka, T. Shimakawa, T. Miyata, and H. Sato. High-Efficiency Oxide Heterojunction Solar Cell Using Cu_2O Sheets, *Japanese Journal of Applied Physics.* 43, 2004, L917-L919.

[32] T. Minami, Y. Nishi, and T. Miyata. Effect of the Thin Ga_2O_3 Layer in n+-ZnO/n-Ga_2O_3/p-Cu_2O Heterojunction Solar Cells, *Thin Solid Films.* 549, 2013, 65-69.

[33] K. Akimoto, S. Ishizuka, M. Yanagita, Y. Nawa, G. K. Paul, and T. Sakurai. Thin film deposition of Cu_2O and application for solar cells, *Solar Energy. 6* 80, 2006, 715-722.

[34] S. Noda, H. Shima, and H. Akinaga. Cu_2O/ZnO Heterojunction Solar Cells Fabricated by Magnetron-Sputtering Deposition Method Films Using Sintered Ceramic Targets, *Journal of Physics: Conference Series. 012027* 433, 2012, 012027.

[35] M. Yang, L. Zhu, Y. Li, L. Cao, and Y. Guo. Asymmetric Interface Band Alignments of Cu_2O/ZnO and ZnO/Cu_2O Heterojunctions, *Journal of Alloys and Compounds.* 578, 2013, 143-147.

[36] R. Jayakrishnan. Photovoltaic Response of Cu_2O/In_2S_3 Hetero-Structure Grown on Cu Substrate, *Materials Science in Semiconductor Processing. 6* 16, 2013, 1608-1612.

[37] C. Jayathialaka, V. Kapakils, W. Siripala, and S. Jayanetti. Improved Efficiency of Electrodeposited p-CuO/n-Cu_2O Heterojunction Solar Cell, *Applied Physics Express.* 8, 2015, 065503.

[38] C. Chao, Y. Ohkura, T. Usui, and J. M. Weisse. Methods for Improving Efficiencies of Cuprous Oxide Solar Cells, .

[39] H. S. Kim, J. W. Lim, S. J. Yun, M. A. Park, S. Y. Park, S. E. Lee, and H. C. Lee. Fabrication and Characterization of Rapidly Oxidized p-Type Cu_2O Films from Cu Films and their Application to Heterojunction Thin Film Solar Cells, *Japanese Journal of Applied Physics.* 52, 2013, 10MB17.

[40] D. O. Scanlon, and G. W. Watson. Undoped n-Type Cu_2O: Fact or Fiction? *The Journal of Physical Chemistry Letters.* 1, 2010, 2582-2585.

[41] W. Siripala, and J. R. P. Jayakody. Observation of n-Type Photoconductivity in Electrodeposited Copper Oxide Film Electrodes in a Photoelectrochemical Cell, *Solar Energy Materials.* 14, 1986, 23-27.

[42] C. A. N. Fernando, P. H. C. de Silva, S. K. Wethasinha, I. M. Dharmadasa, T. Delsol, and M. C. Simmonds. Investigation of n-Type Cu_2O Layers Prepared by Low Cost Chemical Method for Use in Photovoltaic Thin Film Solar Cells, *Renewable Energy.* 26, 2002, 521-529.

[43] C. M. McShane, W. P. Siripala, and K. Choi. Effect of Junction Morphology on the Performance of Polycrystalline Cu_2O Homojunction Solar Cells, *The Journal of Physical Chemistry Letters.* 1, 2010, 2666-2670.

[44] Y. Hsu, J. Wu, M. Chen, Y. Chen, and Y. Lin. Fabrication of Homojunction Cu_2O Solar Cells by Electrochemical Deposition, *Applied Surface Science.* 354, 2015, 8.

[45] Q. Bai, W. Wang, Q. Zhang, and M. Tao. N-Type Doping in Cu_2O with F, Cl, Br: A First-Principles Study, *Journal of Applied Physics.* 11, 2012, 023709.

[46] L. Yu, L. Xiong, and Y. Yu. Cu_2O Homojunction Solar Cells: F-Doped n-Type Thin Film and Highly Improved Efficiency, *Journal of Physical Chemistry.* 119, 2015, 22803-22811.

[47] L. Papadimitriou, and N. A. Economou. Heterojunction Solar Cells on Cuprous Oxide, *Solar Cells.* 3, 1981, 73-80.

[48] V. Georgieva, and M. Ristov. Electrodeposited Cuprous Oxide on Indium Tin Oxide for Solar Applications, *Solar Energy Materials and Solar Cells. 1* 73, 2002, 67-73.

[49] K. Han, and T. Meng. Electrochemically Deposited p-n Homojunction Cuprous Oxide Solar Cells, *Solar Energy Materials & Solar Cells.* 93, 2009, 153-157.

[50] T. Minami, Y. Nishi, T. Miyata, and J. Nomoto. High-Efficiency Oxide Solar Cells with ZnO/Cu_2O Heterojunction Fabrication on Thermally Oxidized Cu_2O Sheets. *Applied Physics Express.* 4, 2011, 062301.

[51] S. Hussain, C. Cao, Z. Usman, Z. Chen, G. Nabi, W. S. Khan, Z. Ali, F. K. Butt, and T. Mahmood. Fabrication and Photovoltaic Characteristics of Cu_2O/TiO_2 Thin Film Heterojunction Solar Cell, *Thin Solid Films.* 522, 2012, 430-434.

[52] C. Tsai, C. Chen, P. Fei, and Y. Hsu. Novel Semiconductor-Liquid Heterojunction Solar Cells Based on Cuprous Oxide and Iodine Electrolyte, *Electrochimica Acta.* 167, 2015, 112-118.

[53] N. G. Elfadill, M. R. Hashim, K. M. Chahrour, M. A. Qaeed, and M. Bououdina. The Influence of Cu_2O Crystal Structure on the Cu_2O/ZnO Heterojunction Photovoltaic Performance, *Superlattices and Microstructures.* 85, 2015, 908-917.

[54] A. O. Musa, T. Akomolafe, and M. J. Carter. Production of Cuprous Oxide, a Solar Cell Material, by Thermal Oxidation and a Study of its Physical and Electrical Properties, *Solar Energy Materials and Solar Cells. 3–4* 51, 1998, 305-316.

[55] G. A. Adegboyega. An Investigation of Copper Oxide Films for Photovoltaic Applications, *Solar & Wind Technology. 3-4* 2, 1985, 191-194.

[56] Z. Rosenstock, and I. Riess. Preparation of Oxide Thin Films by Controlled Diffusion of Oxygen Atoms, *Solid State Ionics.* 136-137, 2000, 921-926.

[57] S. C. Ray. Preparation of Copper Oxide Thin Film by the Sol–gel-like Dip Technique and Study of their Structural and Optical Properties, *Solar Energy Materials and Solar Cells. 3–4* 68, 2001, 307-312.

[58] D. S. C. Halin, I. A. Talib, M. A. A. Hamid, and A. R. Daud. Characterization of Cuprous Oxide Thin Films on n-Si Substrate Prepared by Sol-Gel Spin Coating, *Journal of Solid State Technology and Science. 1* 16, 2008, 232-237.

[59] O. Akhavan, H. Tohidi, and A. Z. Moshfegh. Synthesis and Electrochromic Study of Sol–Gel Cuprous Oxide Nanoparticles Accumulated on Silica Thin Film, *Thin Solid Films. 24* 517, 2009, 6700-6706.

[60] D. S. C. Halin, I. A. Talib, and A. R. Daud. The Effect of Spin Coating Rate on Morphology and Optical Properties of Cuprous Oxide Thin Film Prepared by Sol-Gel Technique, *Journal of the Australian Ceramic Society. 1* 46, 2010, 41-45.

[61] T. D. Golden, M. G. Shumsky, Y. Zhou, R. A. VanderWerf, R. A. Van Leeuwen, and J. A. Switzer. Electrochemical Deposition of Copper (I) Oxide Films, *Chemistry of Materials.* 8, 1996, 2499-2504.

[62] L. Wan, Z. Wang, Z. Yang, W. Luo, Z. Li, and Z. Zou. Modulation of Dendrite Growth of Cuprous Oxide by Electrodeposition, *Journal of Crystal Growth.* 312, 2010, 3085-3090.

[63] Y. Gu, X. Su, Y. Du, and C. Wang. Preparation of Flower-Like Cu_2O Nanoparticles by Pulse Electrodeposition and Their Electrocatalytic Application, *Applied Surface Science.* 256, 2010, 5862-5866.

[64] L. C. Liau, Y. Lin, and Y. Peng. Fabrication Pathways of p-n Cu_2O Homojunction Films by Electrochemical Deposition Processing, *The Journal of Physical Chemistry. 50* 117, 2013, 26426-26431.

[65] J. Xue, Q. Shen, W. Liang, X. Liu, L. Bian, and B. Xu. Preparation and Formation Mechanism of Smooth and Uniform Cu_2O Thin Films by Electrodeposition Method, *Surface and Coatings Technology.* 216, 2013, 166-171.

[66] Q. Li, M. Xu, H. Fan, H. Wang, B. Peng, C. Long, and Y. Zhai. Dielectric Properties Investigation of Cu_2O/ZnO Heterojunction Thin Films by Electrodeposition, *Materials Science and Engineering: B. 8* 178, 2013, 496-501.

[67] S. Laidoudi, A. Y. Bioud, A. Azizi, G. Schmerber, J. Bartringer, S. Barre, and A. Dinia. Growth and Characterization of Electrodeposited Cu_2O Thin Films, *Semiconductor Science and Technology.* 28, 2013, 115005.

[68] M. Majumder, I. Biswas, S. Pujaru, and A. K. Chakraborty. Cuprous Oxide Thin Films Grown by Hydrothermal Electrochemical Depostion Technique, *Thin Solid Films.* 589, 2015, 741-749.

[69] R. M. Brady, and R. C. Ball. Fractal Growth of Copper Electrodeposits, *Nature. 5965* 309, 1984, 225-229.

[70] C. M. Lopez, and K. Choi. Electrochemical Synthesis of Dendritic Zinc Films Composed of Systematically Varying Motif Crystals, *Langmuir.* 22, 2006, 10625-10629.

[71] A. Osherov, C. Zhu, and M. J. Panzer. Role of Solution Chemistry in Determining the Morphology and Photoconductivity of Electrodeposited Cuprous Oxide Films, *Chemistry of Materials.* 25, 2013, 692-698.

[72] W. Zhoa, W. Fu, H. Yang, C. Tian, M. Li, L. Yixing, L. Zhang, Y. Sui, X. Zhou, H. Chen, and C. Zou. Electrodeposition of Cu_2O films and Their Photoelectrochemical Properties, *Crystal Engineering Communications.* 13, 2011, 2871-2877.

[73] E. W. Bohannan, M. G. Shumsky, and J. A. Switzer. Epitaxial Electrodeposition of Copper (I) Oxide on Single-Crystal Gold (100), *Chemistry of Materials.* 11, 1999, 2289-2291.

[74] M. E. Messing, K. Hillerich, J. Johansson, K. Deppert, and K. A. Dick. The Use Of Gold For Fabrication Of Nanowire Structures, *Gold Bulletin. 3* 42, 2009, 172-188.

[75] K. Nakaoka, and K. Ogura. Electrochemical Preparation of p-Type Cupric and Cuprous Oxides on Platinum and Gold Substrates from Copper (II) Solutions with Varous Amino Acids, *Journal of The Electrochemical Society. 11* 149, 2002, C579-C585.

[76] W. Wang, L. Lyu, and M. H. Huang. Investigation of the Effects of Polyhedral Gold Nanocrystal Morphology and Facets on the Formation of Au-Cu_2O Core-Shell Heterostructure, *Chemistry of Materials.* 23, 2011, 2677-2684.

[77] C. Uihlein, D. Frohlich, and R. Kenklies. Investigation of Exciton Fine Structure in Cu_2O, *Physical Review B. 6* 23, 1981, 2731-2740.

[78] B. Balamurugan, and B. R. Mehta. Optical and Structural Properties of Nanocrystalline Copper Oxide Thin Films Prepared by Activated Reactive Evaporation, *Thin Solid Films.* 396, 2001, 90-96.

[79] Y. S. Jeong, H. Kim, and H. S. Lee. Growth and Characterization of p-Cu_2O/n-ZnO Nanorod Heterojunctions Prepared by a Two-step Potentiostatic Method, *Journal of Alloys and Compounds.* 573, 2013, 163-169.

[80] M. Heinemann, B. Eifert, and C. Heiliger. Band Structure and Phase Stability of the Copper Oxides Cu_2O, CuO, and Cu_4O_3, *Physical Review B.* 87, 2013, 115111.

[81] B. K. Meyer, A. Polity, D. Reppin, M. Becker, P. Hering, P. J. Klar, T. Sandar, C. Reindl, J. Benz, M. Eickhoff, C. Heiliger, M. Heinemann, J. Blasing, A. Krost, S. Shokovets, C. Muller, and C. Ronning. Binary Copper Oxide Semiconductors: From Materials Toward Devices, *Physica Status Solidi B. 8* 249, 2012, 1487-1509.

[82] J. Tauc, R. Grigorovici, and A. Vancu. Optical Properties and Electronic Structure of Amorphous Germanium, *Phys Status Solidi.* 15, 1966, 627-637.

[83] "Faraday's Law." *Electronics Inc. A California Corporation.* 2013.Web. <http://www.electrolytics.org/faradaysLaw.html>.

[84] D. E. Aspnes, S. M. Kelso, R. A. Logan, and R. Bhat. Optical Properties of $Al_xGa_{1-x}As$, *Journal of Applied Physics.* 60, 1986, 754.

[85] D. P. Birnie, and J. B. Coulter. *Unpublished* .

[86] W. Wang, D. Wu, Q. Zhang, L. Wang, and M. Tao. pH-Dependence of Conduction Type in Cuprous Oxide Synthesized from Solution, *Journal of Applied Physics.* 107, 2010, .

[87] A. Du Pasquier, Z. Duan, N. Pereira, and Y. Lu. Cuprous Oxide Solution Preparation and Application to Cu_2O-ZnO Solar Cells, *ECS Transactions.* 28, 2010, 179-190.